Chapter 4

Result and Discussion

4.1 Characterization of Y Typed Zeolite

4.1.1 Influence of Aging and Crystallization Time on Zeolite NaY Formation

In this method, sources of silica, alumina, sodium hydroxide and water are combined with aged alumino-silicate nucleation centers. The influence of aging and crystallization times on zeolite formation was investigated. The results are compiled in Table 4.1.

4.1.1.1 Without Aging Step of Nucleation Centers

Without aging step, change of solid phases during various crystallization time are summarized as follows :

Table 4.1 : Results of synthesis of zeolite NaY

Sample number	**Aging time** *at RT, (day)*	**Crystallization time** *at 100 °C, (h)*	**Solid phase**
E01	0	17	Amorphous
E02	0	40	Amorphous + **NaY**
E03	0	90	**NaY** + Other crystalline phase + Amorphous
E04	0	120	**NaY** + Other crystalline phase + Amorphous
E11	1	17	Amorphous
E12	1	40	Amorphous + **NaY**
E13	1	65	**NaY** + Other crystalline phase + Amorphous
E14	1	90	**NaY** + Other crystalline phase
E21	2	17	Amorphous
E22	2	65	**NaY** + Amorphous
E23	2	90	**NaY** + Other zeolites

Table 4.1(continuous)

Sample number	Aging time *at RT, (day)*	Crystallization time *at 100 °C, (h)*	Solid phase
E31	3	17	Amorphous
E32	3	40	Amorphous + **NaY**
E33	3	47	**NaY** + Other crystalline phase
E34	3	65	**NaY** + Other crystalline phase
E41	4	17	Amorphous + **NaY**
E42	4	40	**NaY**
E43	4	65	**NaY**
E44	4	90	**NaY** + Other crystalline phase
E51	5	17	Amorphous + **NaY**
E52	5	40	**NaY**
E53	5	65	**NaY**
E54	5	90	**NaY** + Other crystalline phase
E221	22	17	Amorphous + **NaY**
E222	22	40	**NaY**
E223	22	65	**NaY**

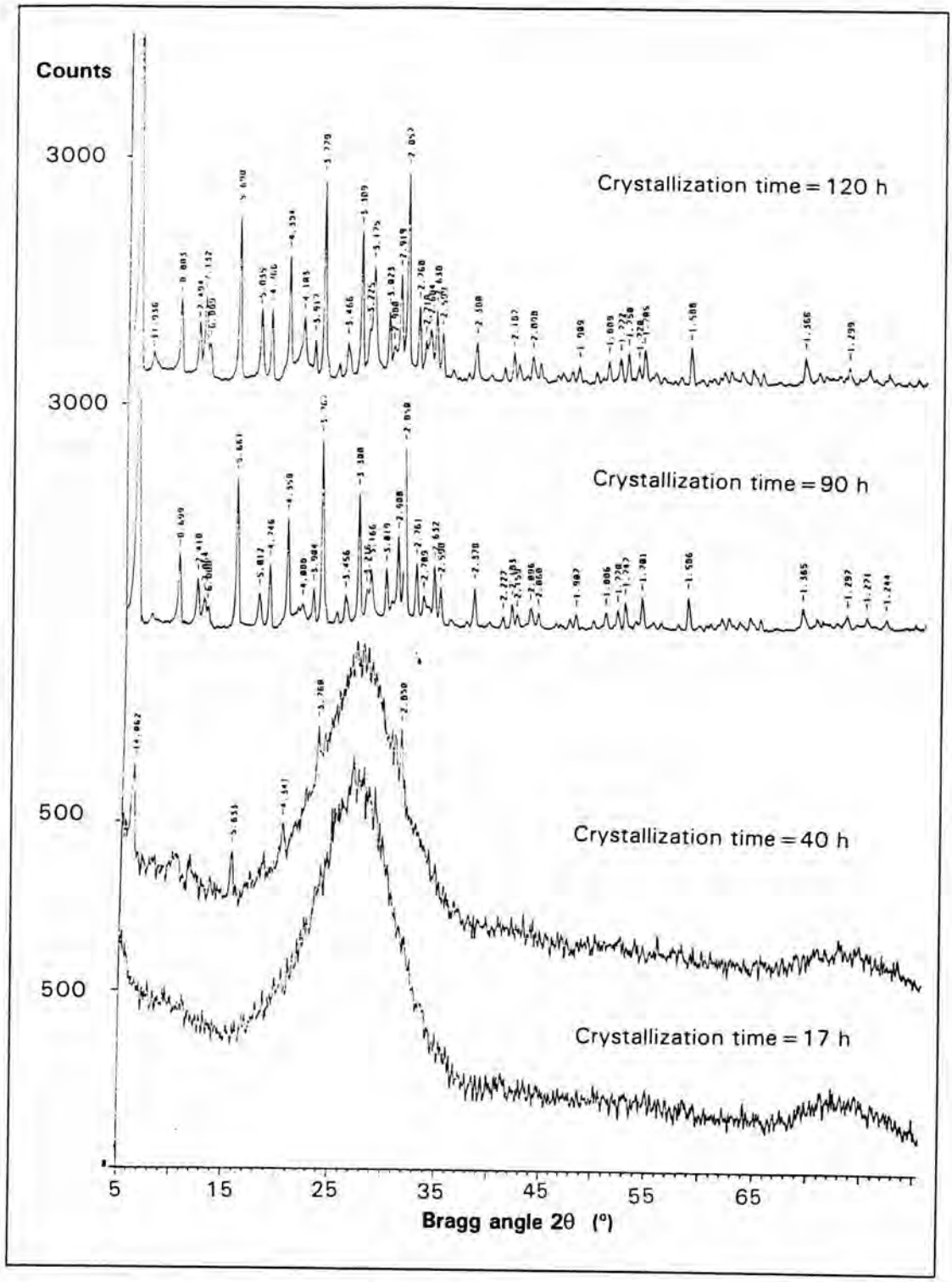

Figure 4.1 : XRD patterns of zeolite products at various crystallization time without aging step.

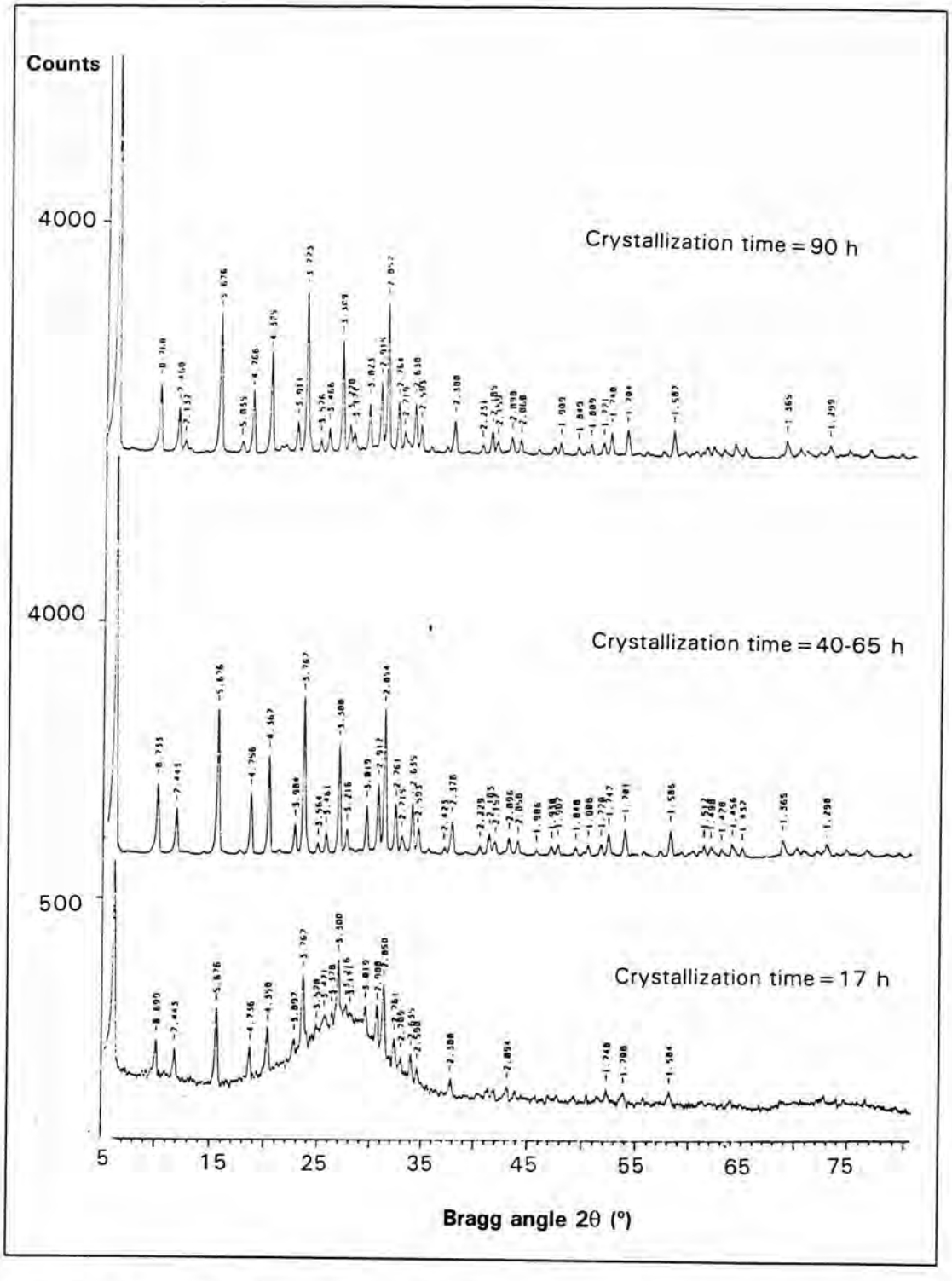

Figure 4.2 : XRD patterns of zeolite products at various crystallization time after aging the nucleation centers for at least 4 days.

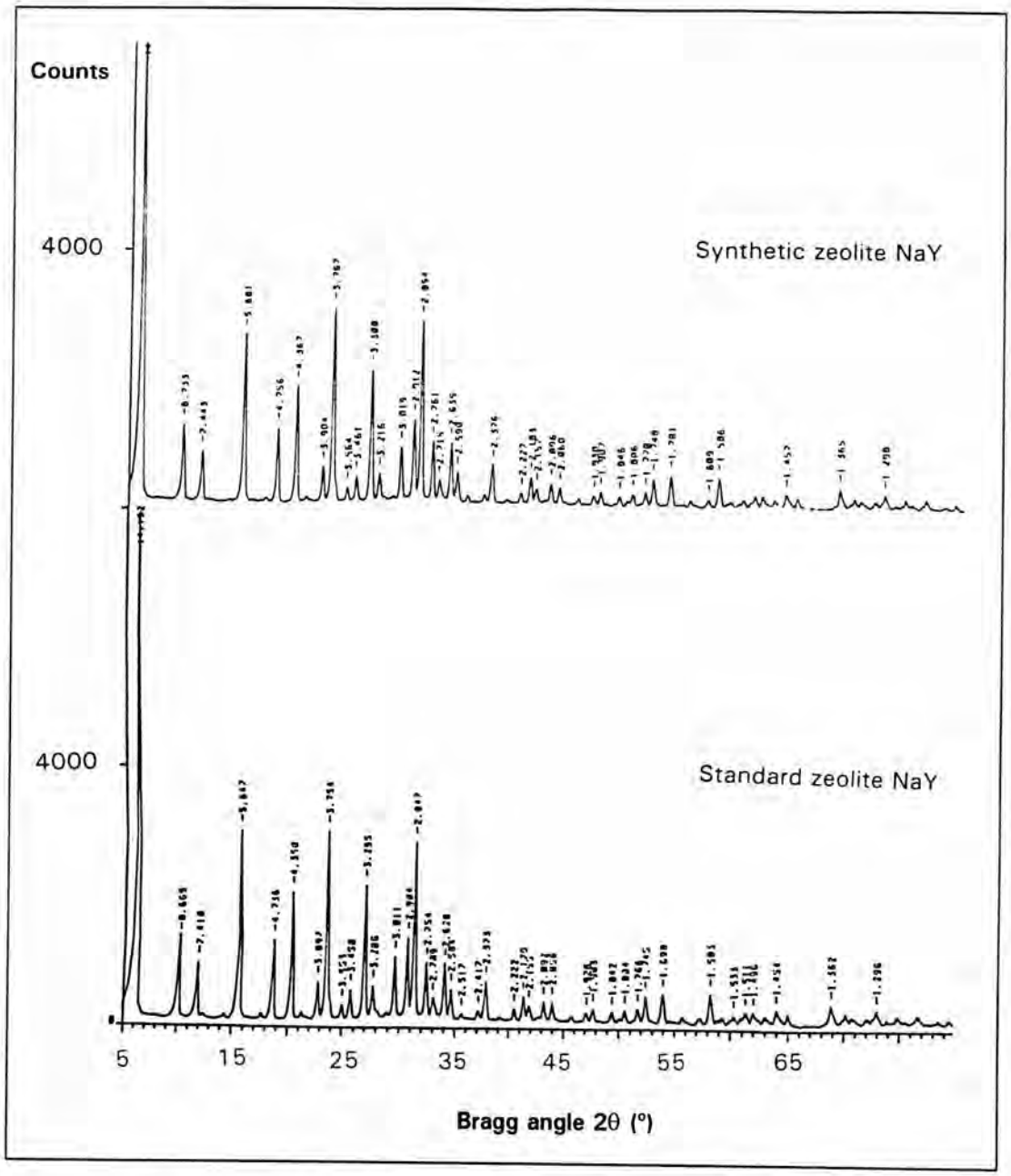

Figure 4.3 : XRD patterns of synthetic zeolite NaY from this process and standard zeolite NaY from Aldrich.

(i) After 17 h only amorphous phase is observed in the solid product.

(ii) After 40 h amorphous phase is the major part with the little appearance of a crystalline phase.

(iii) After 90 h most amorphous phase disappears while the crystalline phase of zeolite NaY becomes predominant. Another crystalline phase (shaded peaks) also appears as a by product.

(iv) After 120 h intensities of the by-product crystalline phase increase drastically.

Zeolite Y is metastable phase which can transform to other phases under this crystallization condition. All conditions without aging the slurry of nucleation centers provide solid impurities in the form of either amorphous phase or crystalline phase. In next section, we increase aging time to improve the condition in the synthesis of zeolite Y.

4.1.1.2 With Aging Step of the Nucleation Centers for 1-3 Days

Upon aging the aluminosilicate gel of nucleation centers over a period of about 1-3 days, the crystalline phase of zeolite NaY still contains undesirable impurities of other crystalline or amorphous phase or both. These experiments demonstrate that the conditions are not suitable for the production of synthetic zeolite NaY with high crystallinity.

4.1.1.3 With Aging Step of the Nucleation Centers for at least 4 Days

After aging the aluminosilicate gel for at least 4 days, the results of the crystallization of zeolite NaY which were followed by XRD (Figures 4.2 and 4.3) are summarized as :

(i) Less than 40 h amorphous phase is still present with the crystalline phase of zeolite NaY. Longer crystallization time reduces the amount of amorphous phase.

(ii) Only zeolite NaY product is formed when the crystallization time is at least 40 hours but not more than 65 hours.

(iii) The overlong crystallization time (>65 hours) results in the increase of the undesired crystalline phase other than zeolite NaY.

This process is evident that including the room-temperature aging step of the nucleation centers can improve the formation of high crystalline zeolite NaY. The optimum reaction time under the conditions employed in this work was found to include the aging time of the diluted nucleation centers $16.2Na_2O:1.2Al_2O_3:15SiO_2:640H_2O$ at least 4 days and crystallization time of the reactant mixture $1.9Na_2O:Al_2O_3:6SiO_2:100H_2O$ added with the nucleation centers about 40-65 hours.

4.1.2 Percent Crystallinity and XRF Analysis of the Zeolite NaY

The synthetic zeolite NaY from this work has 97 % crystallinity and similar characteristic XRD pattern as that of standard zeolite NaY. The crystallinity of zeolite NaY is shown in Figure 4.4. The method for determining the percent crystallinity is calculated by :

$$\% \text{ Crystallinity} = (\Sigma I_U / \Sigma I_S) \times 100 \qquad \ldots(4.1)$$

Here ΣI_U and ΣI_S represent the sum of characteristic peak intensity of unknown (synthetic zeolite NaY) and of standard (zeolite NaY from Aldrich) at Bragg's angle 2θ of 10.1, 11.9, 15.6, 18.6, 20.3, 23.6, 27.0 and 31.3 in XRD data. The result shows that the product synthesized in this work has high crystallinity. At this point, it should be remined that different standards may have different levels of crystallinity.

XRF analysis showed that the silica/alumina ratio of the zeolite NaY product is 4.6 and expressed in terms of structural formula as follows :

$$Na_{58}.[(AlO_2)_{58}.(SiO_2)_{134}].\ 235H_2O$$

The determination of the formula is based on the concept that the summation of tetrahedron atoms in faujasite structure must be 192 atoms.

$$Al + Si = 192 \quad ...(4.2)$$

From analysis, $SiO_2/Al_2O_3 = 4.6$ ...(4.3)

$$\text{or } Si/Al = 2.3 \quad ...(4.4)$$

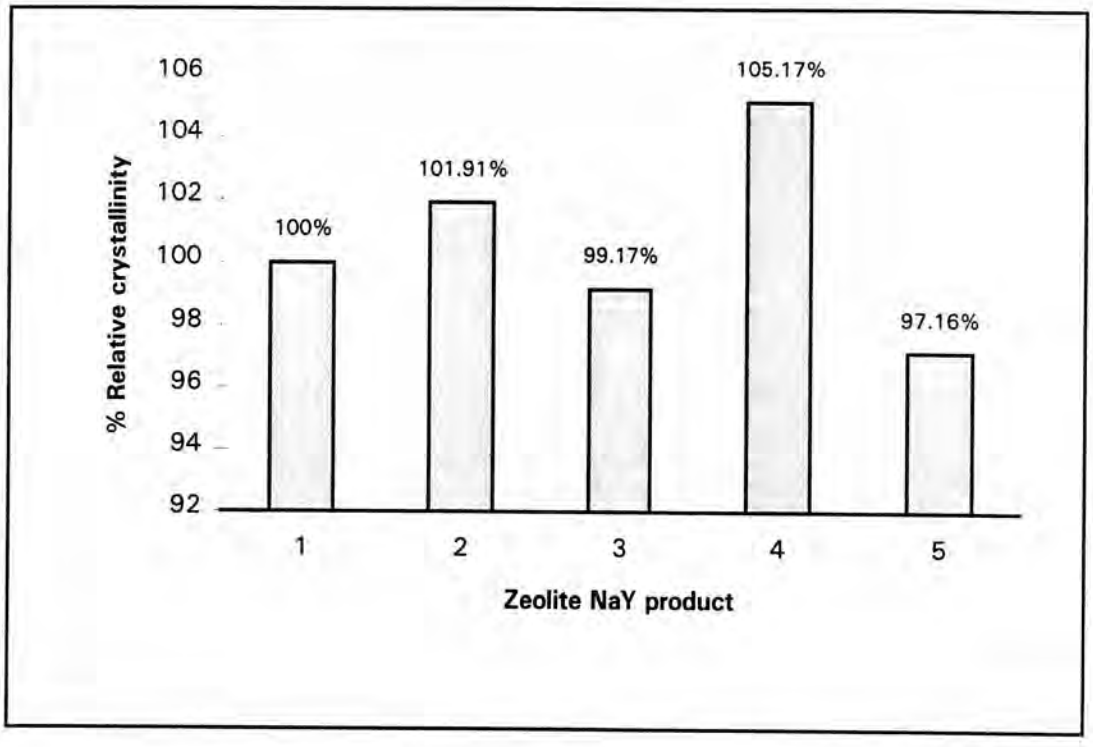

Figure 4.4 : Percent crystallinity of zeolite NaY : 1 = Standard zeolite NaY; 2 = Aging time 4 days and crystallization time 40 h; 3 = Aging time 4 days and crystallization time 65 h; 4 = Aging time 5 days and crystallization time 40 h; 5 = Aging time 5 days and crystallization time 65 h.

4.1.3 Ammonium Form and Hydrogen Form of the Zeolite Y

To prepare zeolite HY, indirect method was carried out via ammonium exchange of zeolite NaY and subsequent deammination at elevated temperature leaving protons as the new cations of the zeolite. After exchange the zeolite NaY with the solution of NH_4Cl, the zeolite was characterized using infrared spectroscopy. The infrared spectra of the zeolite before and after the ammonium exchange process are shown in Figures 4.5 and 4.6, respectively. In Figure 4.6 new absorption bands near 3400 to 3000 cm^{-1} and at 1450 cm^{-1} are characteric bands of N-H stretching and N-H bending vibrations, respectively. These bands did not appear in the spectrum of the zeolite NaY (Figure 4.5). This indicates the presence of NH_4^+ ion in the zeolite Y after the ion exchange. Each spectrum shows one band at 1640 cm^{-1} which is assigned to moisture adsorbed in zeolite pores. Other bands between 1250-300 cm^{-1} are assigned to the fundamental vibrations of the zeolite framework[31] which are summarized in Table 4.2.

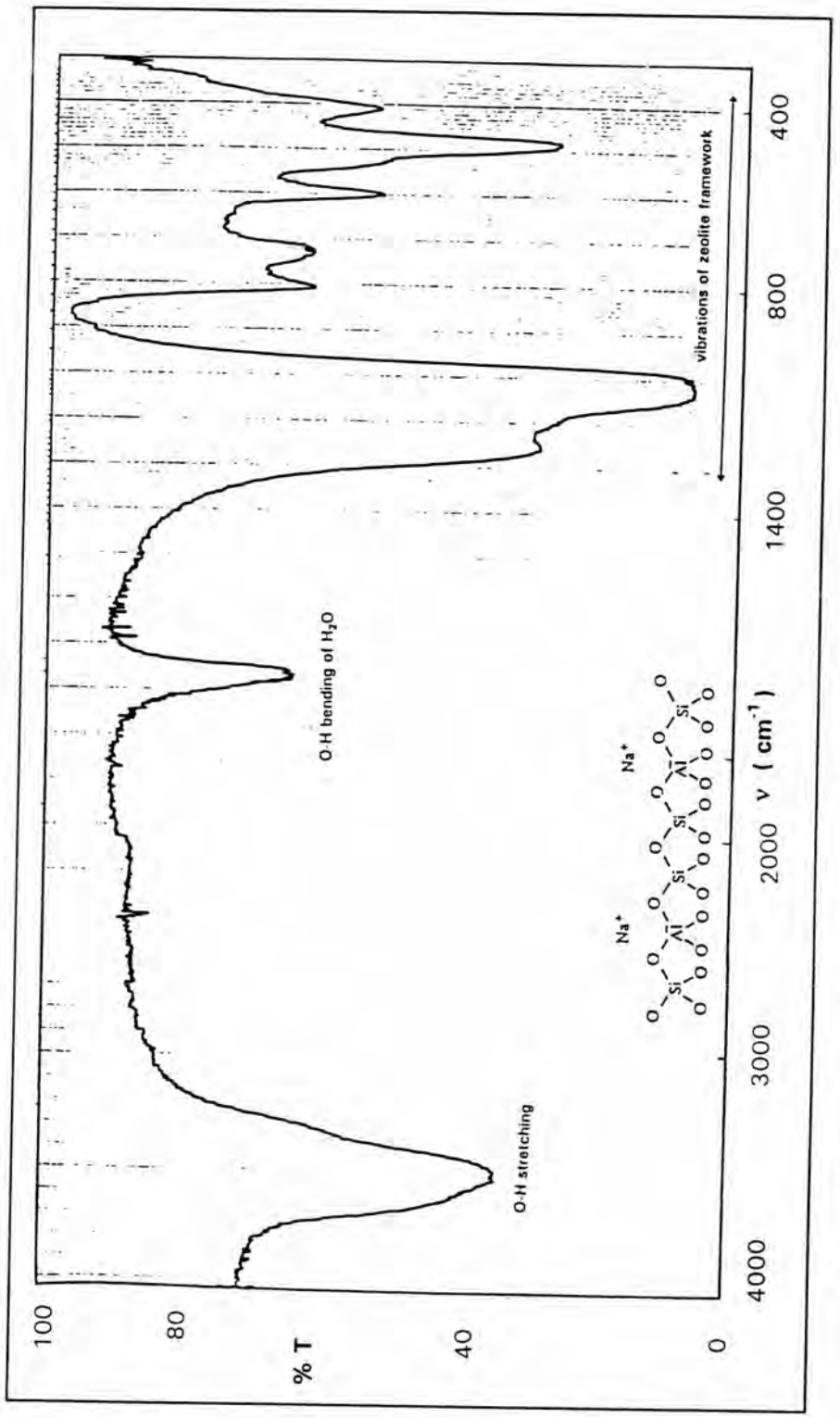

Figure 4.5 : IR spectrum of zeolite NaY before ammonium exchange process.

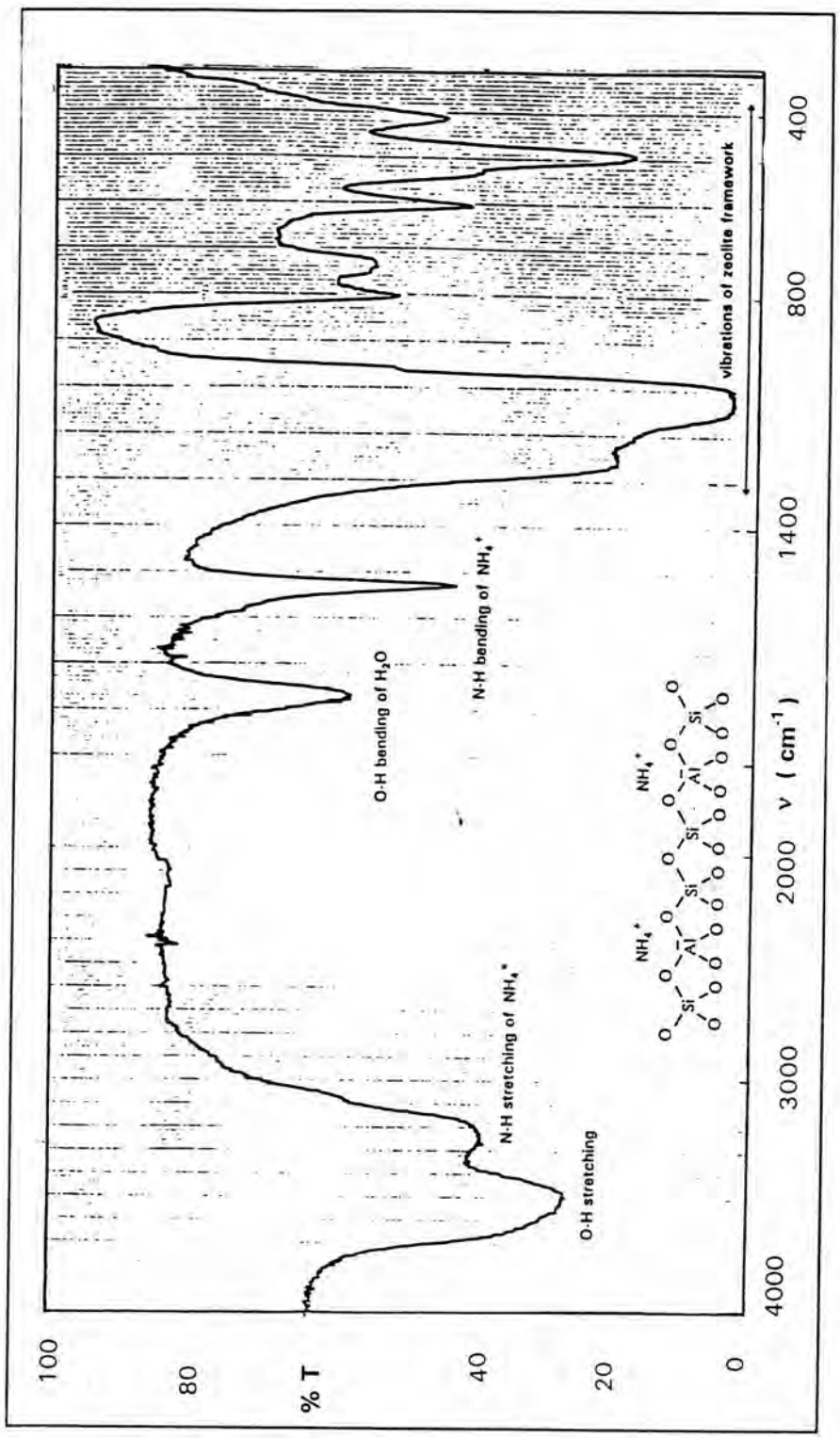

Figure 4.6 : IR spectrum of zeolite NH_4Y obtained from the ammonium exchange process of zeolite NaY.

Table 4.2 : IR assignments of the zeolite framework.

Internal tetrahedra (structure insensitive)		**External linkages** (structure sensitive)	
asym. stretch	1250-950 cm^{-1}	asym. stretch	1050-1150 cm^{-1}
sym. stretch	720-650 cm^{-1}	sym. stretch	750-820 cm^{-1}
T-O bend	420-500 cm^{-1}	double ring	650-500 cm^{-1}
		pore opening	300-420 cm^{-1}

The XRD patterns of the zeolite NH_4Y and the zeolite NaY (Figure 4.7) are similar. This means that the zeolite Y retains its structure after the ion exchange process.

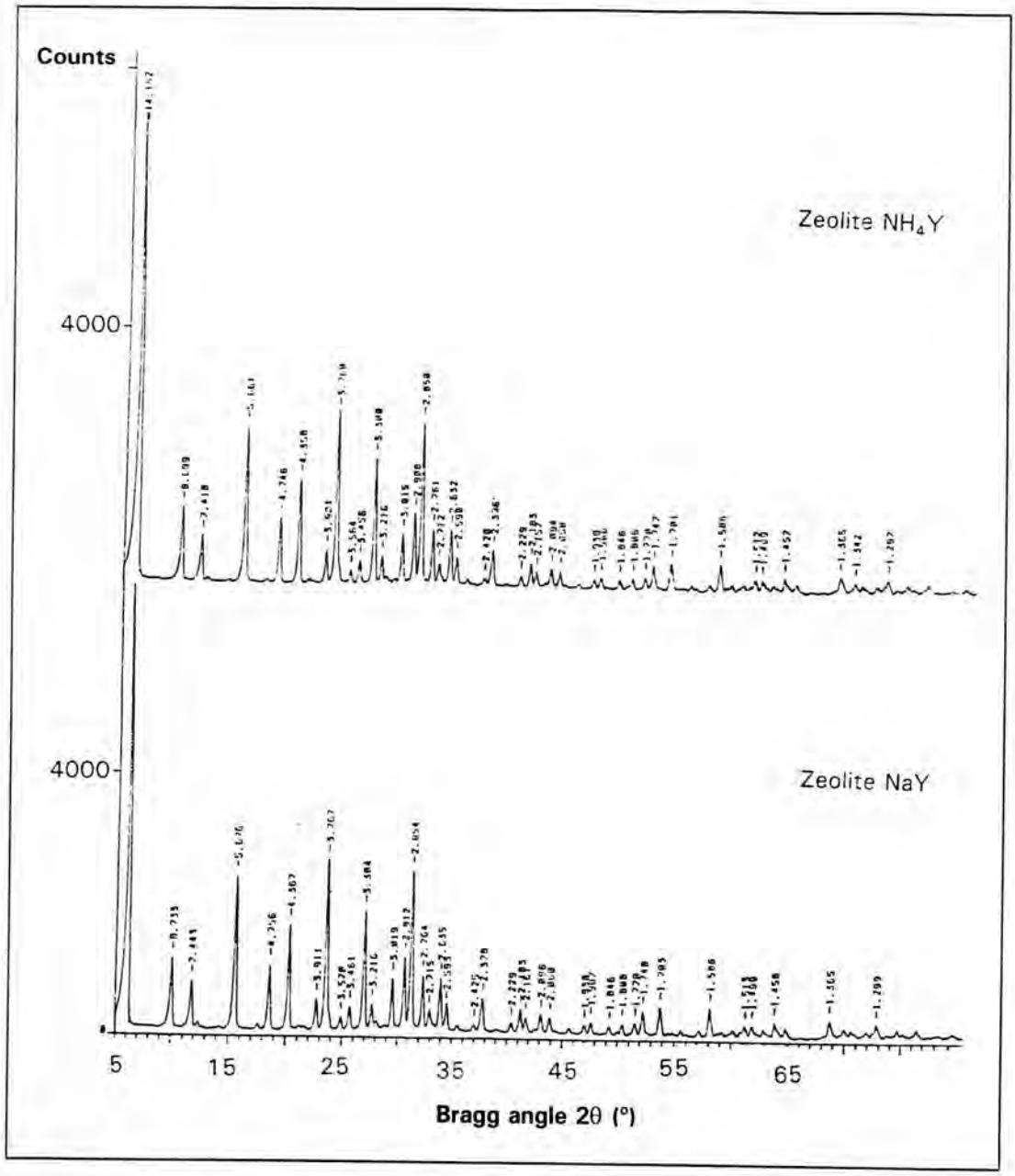

Figure 4.7 : XRD patterns of zeolites NaY and NH_4Y obtained from the NH_4^+ exchange process of the zeolite NaY.

4.2 Characterization of the Zeolite NaY Loaded $Rh(acac)(CO)_2$

4.2.1 IR Spectroscopy of the Zeolite NaY Loaded $Rh(acac)(CO)_2$

The infrared spectrum of the greenish-gray zeolite NaY loaded $Rh(acac)(CO)_2$ shows three strong terminal carbonyl bands (Figure 4.8 and Table 4.3). The presence of green color is a sign of the unreacted precursor. The gray means that a new product is formed.

Table 4.3 : IR data of the zeolite NaY loaded $Rh(acac)(CO)_2$

Complex	ν_{CO} (cm^{-3})
$Rh(acac)(CO)_2$ precursor	2085s, 2065m, 2013s, 1987m
Zeolite NaY loaded $Rh(acac)(CO)_2$	2103s, 2032s, 2013s

A comparison with the spectrum of $Rh(acac)(CO)_2$ precusor shows that the shift of the terminal carbonyl bands to higher wavenumber at 2103 and 2032 cm^{-1} is observed by about 20 cm^{-1}. This shift indicates that replacement of the acac ligand by an oxygen ring of zeolite leads to the decrease of electron density around the rhodium atom. A similar interpretation has been suggested by Ozin et al.[45] for the formation of $Z\text{-}O\text{-}Rh(CO)_2$ as a result of $Rh(acac)(CO)_2$ impregnated into zeolite NaY.

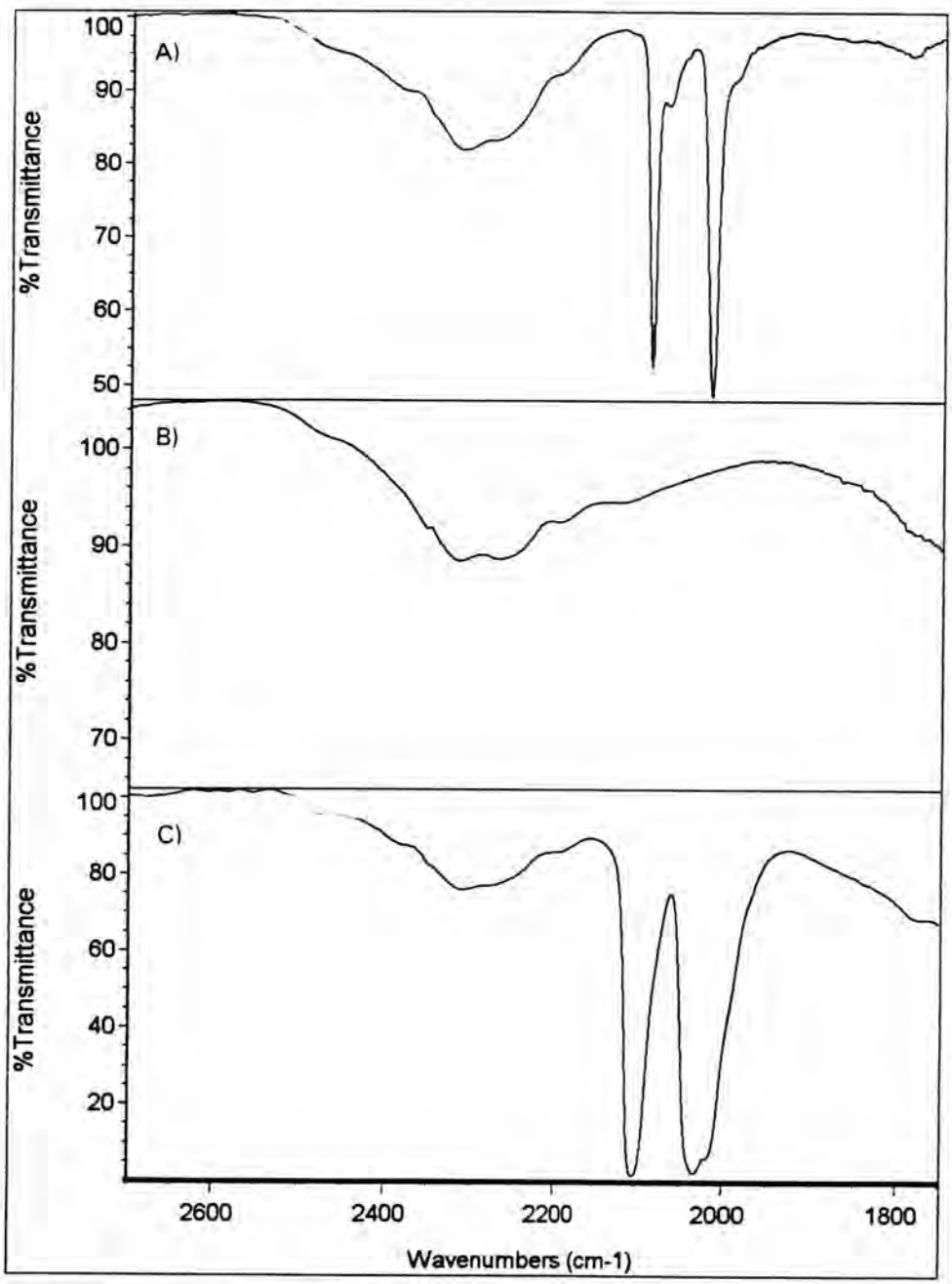

Figure 4.8 : IR spectra : A = $Rh(acac)(CO)_2$ precursor; B = Zeolite NaY; C = Zeolite NaY loaded $Rh(acac)(CO)_2$, all IR samples were pasted in fluorolube.

The IR bands at 2103 and 2039 cm^{-1} are attributed to the production of Z-O-$Rh(CO)_2$ with a concomitant loss of Na(acac).

In contrast, the terminal carbonyl band at 2013 cm^{-1} is at the same position as that of the original $Rh(acac)(CO)_2$ precursor suggesting the presence of unreacted $Rh(acac)(CO)_2$ precursor in zeolite pores. To confirm this result, the obtained product was determined with the thermal treatment, vide infra. No bridging CO bands are observed at lower frequencies, the formation of Rh clusters can thus be neglected. The reaction can be shown in Scheme 4.1.

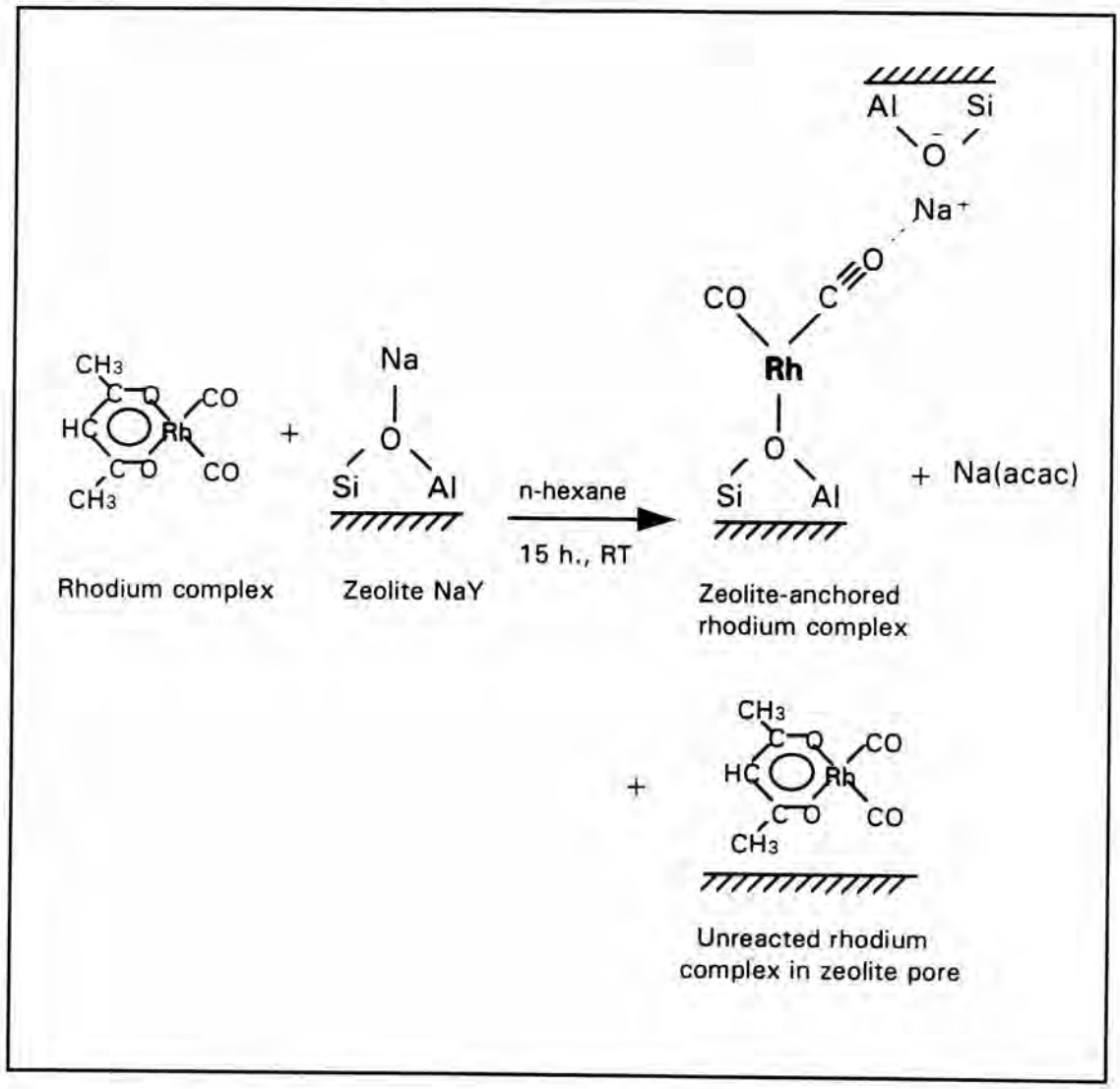

Scheme 4.1 : Proposed reaction of $Rh(acac)(CO)_2$ and the zeolite NaY.

4.2.2 Thermal Stability of the Zeolite NaY Loaded $Rh(acac)(CO)_2$

The IR data of the zeolite NaY loaded $Rh(acac)(CO)_2$ heated under vacuum at 30, 80, 100 and 200 °C are shown in Figure 4.9 and Table 4.4. At 80 and 100 °C, the IR spectra show six bands at 2103s, 2090s, 2070m, 2039s, 2013s and 1990m cm^{-1} due to terminal carbonyl groups. This result shows that the obscured bands are revealed by the decrease of the bands at 2013 and 2039 cm^{-1}. The IR spectrum at 100 °C is not significantly different from the spectrum at 80 °C. At 200 °C both bands at 2103 and 2039 cm^{-1} completely disappeared while the other set of 4 bands at 2090, 2070, 2013 and 1990 cm^{-1} decreases in intensity and finally only the strongest 2090 and 2013 cm^{-1} are retained. It can be deduced that two species are formed in the zeolite NaY loaded $Rh(acac)(CO)_2$ as follows :

(i) The bands at 2103 and 2039 cm^{-1}, marked as ●, are interpreted as Z-O-$Rh(CO)_2$ form in zeolite.

(ii) The bands at 2090s, 2070m, 2013s and 1990m cm^{-1}, marked as ◆, are interpreted as unreacted $Rh(acac)(CO)_2$ in zeolite pore.

The decrease of the CO bands of the two species in the zeolite NaY without new band appearance indicates that the zeolite NaY loaded $Rh(acac)(CO)_2$ decomposes at 80 °C in vacuum while the free precursor

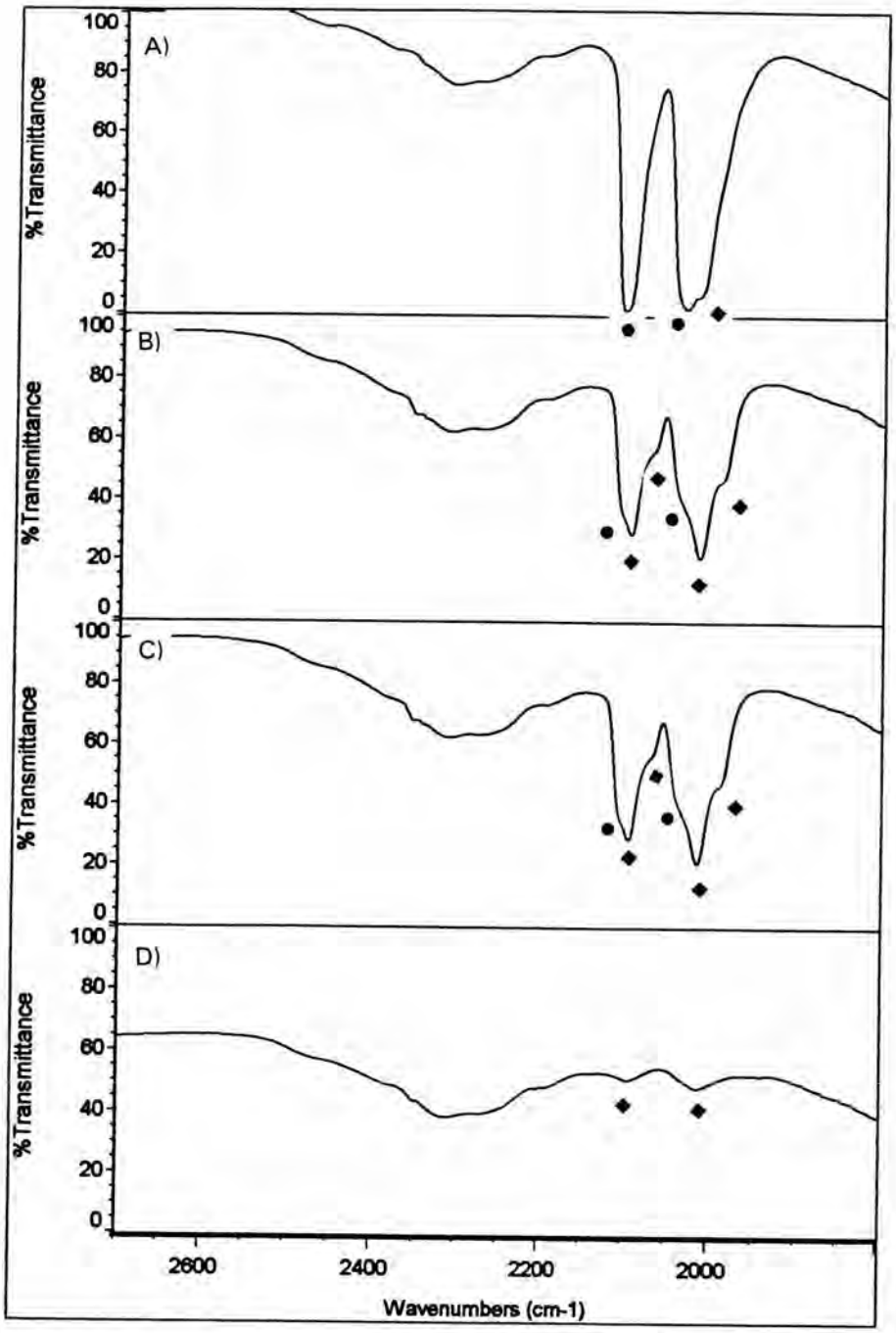

Figure 4.9 : IR spectra for the study of thermal stability of zeolite NaY loaded $Rh(acac)(CO)_2$: A = 30 °C; B = 80 °C; C = 100 °C; D = 200 °C, in vacuum.

sublimes with slight decomposition at 90 °C in vacuum.[46] Therefore, it is less thermally stable than the free $Rh(acac)(CO)_2$ precursor.

Table 4.4 : IR data of the zeolite NaY loaded $Rh(acac)(CO)_2$ heated at different temperatures.

Temperature (°C)	ν_{CO} (cm^{-1})	
	Zeolite-anchored rodium complex (Z-O-$Rh(CO)_2$)	Unreacted rhodium complex in zeolite pore
30	2103, 2039	2013
80	2103(↓), 2039(↓)	2090(↓), 2070(↓), 2013(↓), 1990(↓)
100	2103(↓), 2039(↓)	2090(↓), 2070(↓), 2013(↓), 1990(↓)
200	-	2090, 2013

remarks : ↓ = Decreasing intensity.

4.3 Characterization of the Zeolite HY Loaded $Rh(acac)(CO)_2$

4.3.1 IR Spectroscopy of the Zeolite HY Loaded $Rh(acac)(CO)_2$

The infrared spectrum of the light gray solid zeolite HY loaded $Rh(acac)(CO)_2$ shows two strong terminal carbonyl bands at 2110 and 2044 cm^{-1} (Figure 4.10). The two strong bands shift to higher frequencies which are assigned to Rh dicarbonyl species anchored to the zeolite surface ($Z\text{-}O\text{-}Rh(CO)_2$). This indicates that the acac ligand reacts with a proton of the zeolite to form the H(acac). The H(acac) is expected to be adsorbed on the zeolite, as indicated by th IR bands at 1588 and 1536 $cm.^{-1}$ The replacement of the acac ligand by the zeolite oxygens was confirmed by the decrease of the π-back bonding from Rh to CO ligands and resulting in the CO band shift to higher frequencies. The color of the sample shows no green precursor left in the zeolite. This means that the protons of zeolite Y is more reactive than the sodium ions for anchoring reaction of $Rh(acac)(CO)_2$ to the zeolite surface.These results show that the $Rh(acac)(CO)_2$ precusor can be anchored into the acidic zeolite at room temperature as shown in Scheme 4.2.

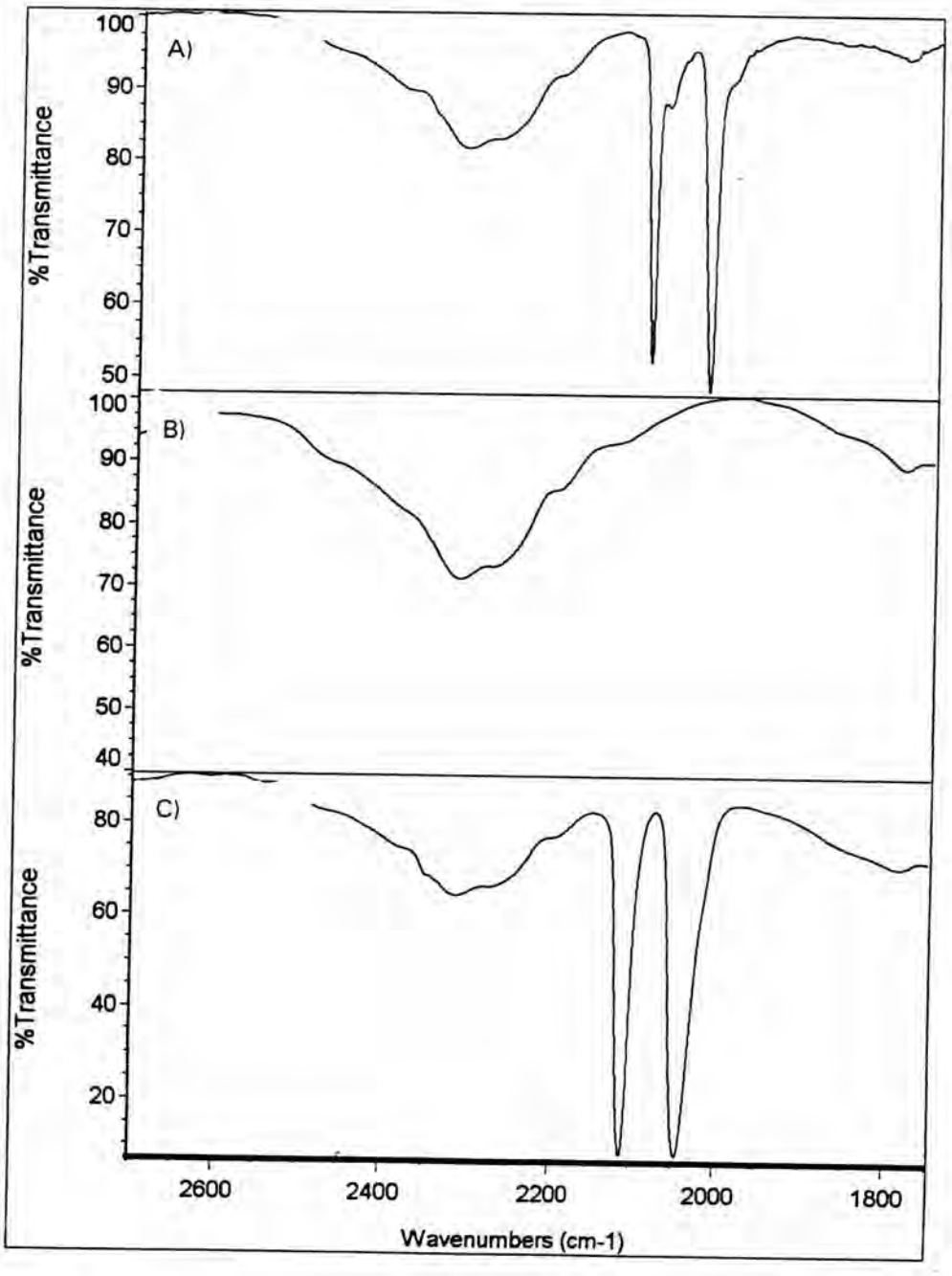

Figure 4.10 : IR spectra : A = $Rh(acac)(CO)_2$ precursor; B = Zeolite HY; C = Zeolite HY loaded $Rh(acac)(CO)_2$, all IR samples are pasted in fluorolube.

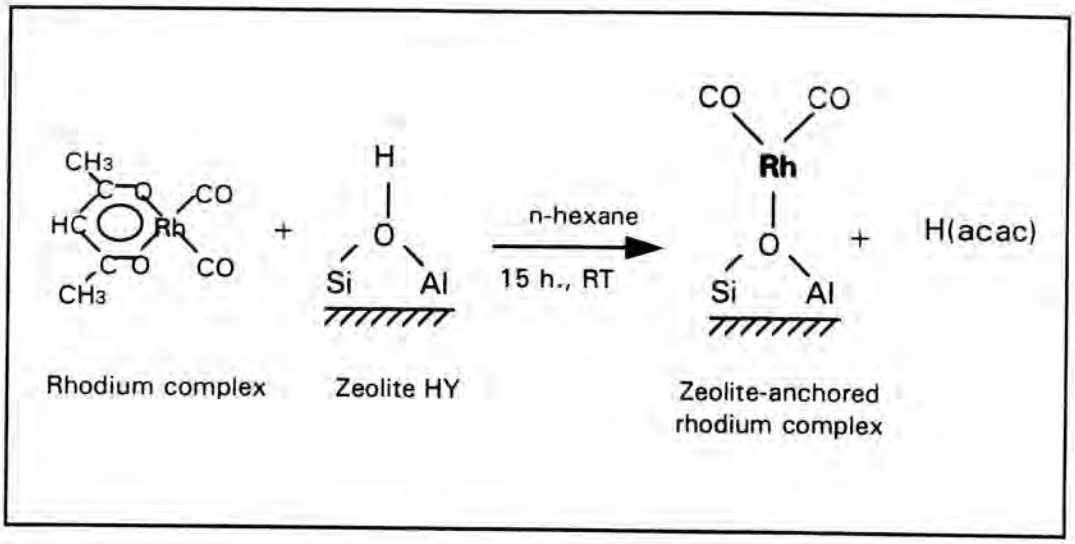

Scheme 4.2 : Proposed reaction of $Rh(acac)(CO)_2$ impregnated into the zeolite HY.

In addition, the IR data of the sample $Rh(acac)(CO)_2$ loaded in the zeolite NaY and the zeolite HY show the carbonyl group interacting with the zeolite sodium cation. The interaction between Na ions and CO ligands (see Scheme 4.1) caused lower symmetry and a weaker CO bond.[47] Therefore, the carbonyl bands of $Z\text{-}O\text{-}Rh(CO)_2$ in zeolite NaY are at lower vibrational frequencies than the carbonyl bands of $Z\text{-}O\text{-}Rh(CO)_2$ in zeolite HY which contains almost no Na ions.

4.3.2 Thermal Stability of the Zeolite HY Loaded $Rh(acac)(CO)_2$

The IR spectra of the zeolite HY loaded $Rh(acac)(CO)_2$ heat in vacuum at 100, 200 and 300 °C are shown in Figure 4.11. It is found that the zeolite-anchored rhodium product is stable up to 200 °C and decomposes upon thermal treatment at 300 °C in vacuum by loss of CO ligands and formation of a new carbonyl stretching band at 2092 cm^{-1}. There are neither other bands belonging to the precursor nor bridging CO bands appearing in the spectrum. The band at 2092 cm^{-1} is thus assigned to a monocarbonyl rhodium species. Zeolite HY loaded $Rh(acac)(CO)_2$ is more thermally stable than the free precusor which sublimes under vacuum at 90 °C with slight decomposition.

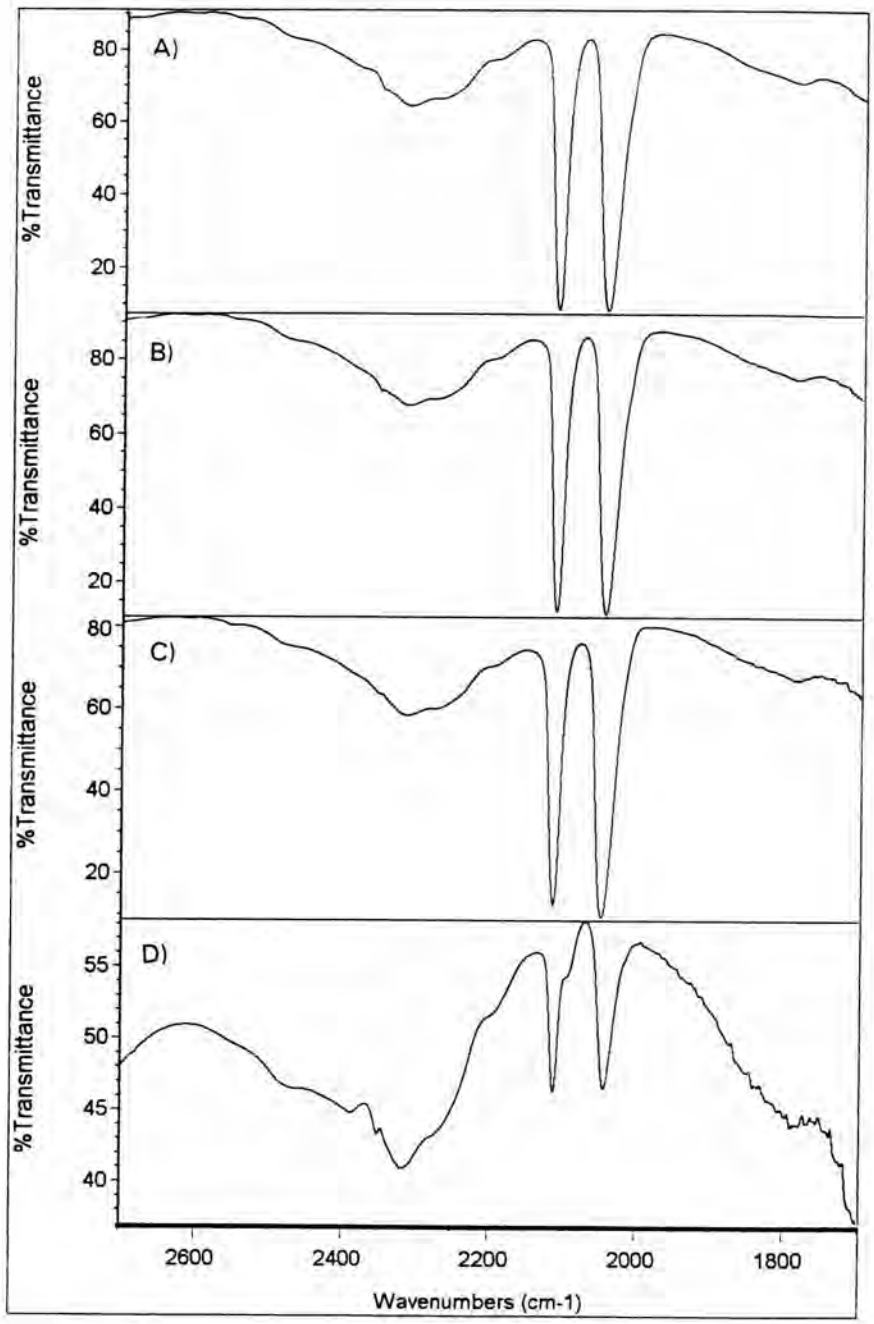

Figure 4.11 : IR spectra for the study of thermal stability of the zeolite HY loaded $Rh(acac)(CO)_2$: A = 30 °C; B = 100 °C; C = 200 °C; D = 300 °C, in vacuum.

4.4 Propylene Hydroformylation

4.4.1 Continuous-Feed System

Under continuous feeds of C_3, H_2, CO and N_2 1.5:2:2:2 at 30, 80 and 120 °C for 2 h, the results of GC analysis for propylene hydroformylation catalyzed by the zeolite HY loaded Rh(acac)$(CO)_2$ are summarized in Table 4.5

Table 4.5: The result for propylene hydroformylation catalyzed by the zeolite HY loaded Rh(acac)$(CO)_2$ in continuous-feed system.

Temperature (°C)	Product	
	Gas phase	Liquid phase
30	nil.	nil.
80	nil.	nil.
120	nil.	nil.

The results show that continuous gas feeds fails to convert propylene to 1-butanal. It is possible either that the products may be trapped in the zeolite pores or that the flow rate of gas feed is too fast; therefore, the contact time between gas molecules and the catalyst in zeolite pores is not enough to initiate the reaction.

Thus the continuous feed apparatus in this project is not suitable for investigation of hydroformylation catalyst. In next section, we design the catalytic apparatus as a batch system.

4.4.2 Batch System Without Vacuum Distillation Technique

The results of GC analysis for propylene hydroformylation catalyzed by the zeolite HY loaded $Rh(acac)(CO)_2$ under the initial mixture of propylene, H_2 and CO at 1:2:2 at ambient pressure and room temperature for 1-5 days are summarized in Tables 4.6 and 4.7.

Table 4.6 : The result for propylene hydroformylation catalyzd by the zeolite HY loaded $Rh(acac)(CO)_2$ in the batch system without vacuum distillation technique

Reaction time (day)	Product in gas phase
1	nil.
2	nil.
3	nil.
4	nil.
5	nil.

Table 4.7 : The result for propylene hydroformylation catalyzed by the zeolite NaY loaded $Rh(acac)(CO)_2$ in the batch system without vacuum distillation technique

Reaction time (day)	Product in gas phase
1	n-hexane (32.55%)
2	n-hexane (32.47%)
3	n-hexane (30.57%)
4	n-hexane (35.74%)
5	n-hexane (31.76%)

Remark : % = % relative peak area in gas chromatograms

The zeolite HY loaded $Rh(acac)(CO)_2$ was catalytically inactive to convert propylene to any product where as the zeolite NaY loaded $Rh(acac)(CO)_2$ was able to convert propylene to n-hexane but not aldehyde in 1 day. This suggests that the zeolite NaY loaded $Rh(acac)(CO)_2$ may act as a hydrogenation catalyst under this condition that leads to the pathway in Scheme 4.3. The competition between hydroformylation and hydrogenation depends on initial addition of CO or H_2 gas to complex 3, $(L)_2Rh(CO)(CH_2CH_2R)$. Using the ratio of $CO:H_2=1:1$ cis-H_2 oxidative addition on the Rh atom is prefered in zeolite pores. This causes

hydrogenation predominant comparing to hydroformylation of 1-hexene and n-hexane was thus found as the major product.

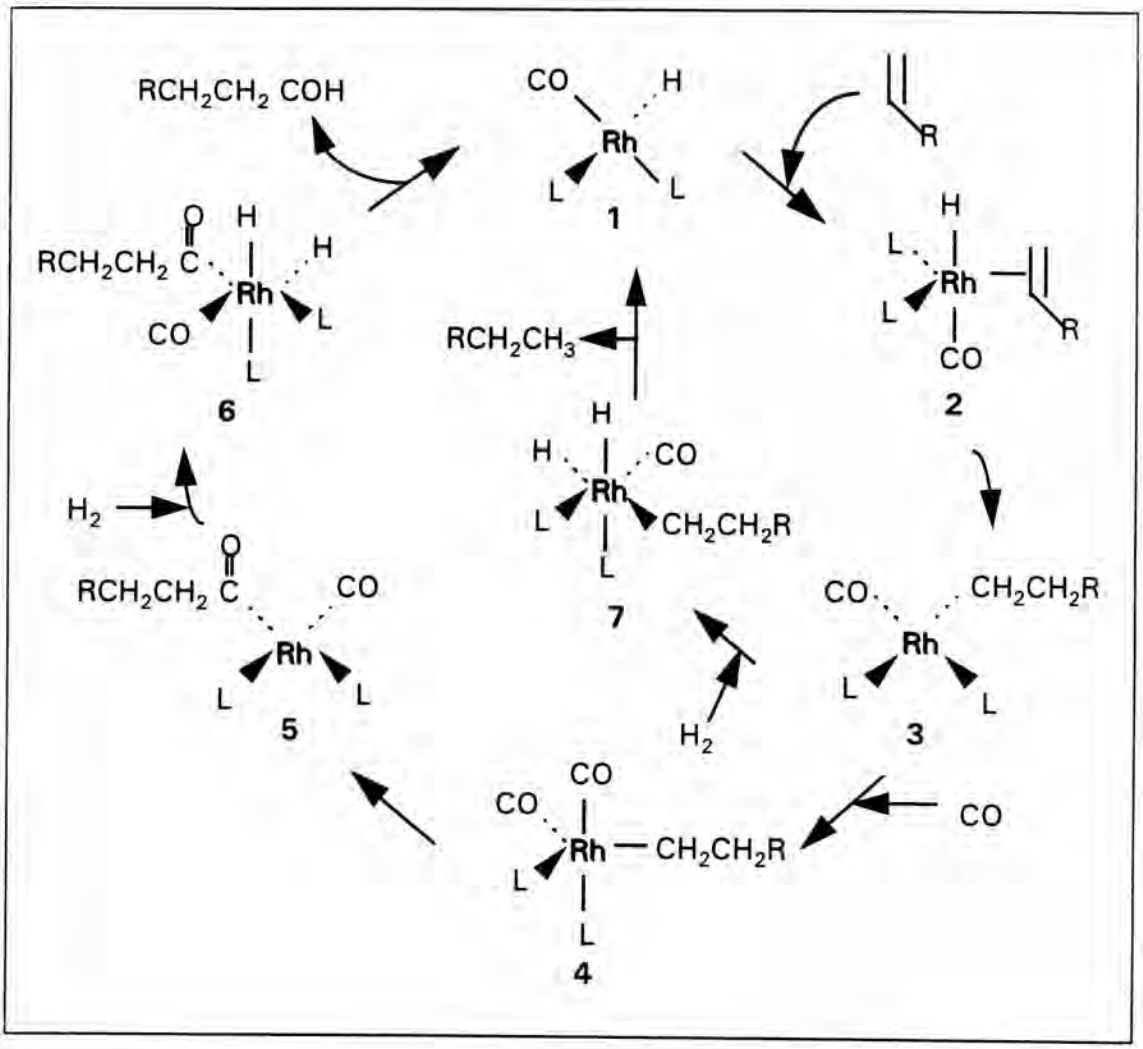

Scheme 4.3 : Possible reaction pathways for hydrogenation of 1-alkene (L may be zeolite framework).

This result implies that the flow rate ratio of C_3:H_2:CO may be inappropriate for propylene conversion to 1-butanal and/or the 1-butanal product may be trapped in the zeolite pores. In next section, we

design apparatus as batch system with vacuum distillation technique to remove adsorbed 1-butanal, if any, from zeolite pores to gas phase and also various flow rate ratio of C_3:CO:H_2 to enhance formation of catalytically active species.

4.4.3 Life Time of Catalysts

The question about life time of the catalyst is interesting ; therefore, the flow rate of C_3:CO:H_2 = 1:2:6 was chosen for investigation of the life time of catalysts.

4.4.3.1 GC Results

The results shown in Figures 4.12 and 4.13 were obtained from the repeated utilization of the zeolite HY loaded Rh(acac)$(CO)_2$ and the zeolite NaY loaded Rh(acac)$(CO)_2$, respectively as catalysts for each five-day reaction time.

Figure 4.12 shows the catalytic run # 1 to 4 for little amount of 1-butanal product and the catalytic run # 5 for the maximum one in gas phase. This may be accounted for adsorptivity of 1-butanal on the polar surface of the zeolite HY at run # 1 to 4. Evacuation at room temperature

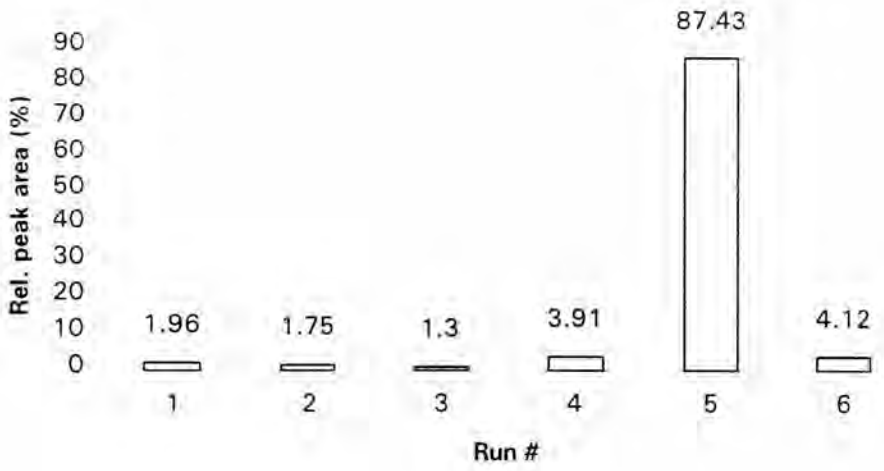

Figure 4.12 : Quantity of 1-butanal in gas phase from propylene hydroformylation with the zeolite HY loaded $Rh(acac)(CO)_2$.

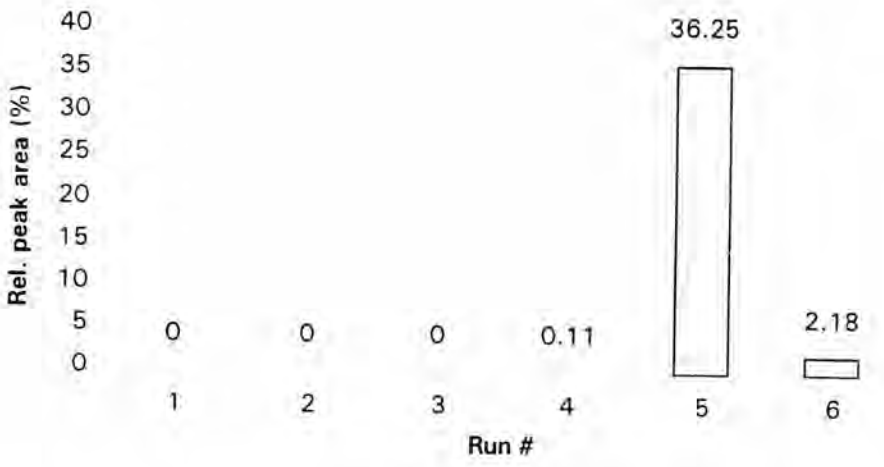

Figure 4.13 : Quantity of 1-butanal in gas phase from propylene hydroformylation with the zeolite NaY loaded $Rh(acac)(CO)_2$.

is not powerful enough to remove 1-butanal from the zeolite pore. After the saturation of adsorption, on the other word beyond its adsorption capacity, the zeolite HY at run # 5 can no longer adsorb excess 1-butanal and then 1-butanal can be removed to the gas phase and observed by GC which is shown in Figure 4.14. The chromatogram of run # 5 for the NaY system is shown in Figure 4.15. Comparing to the HY catalyst, the NaY loaded $Rh(acac)(CO)_2$ catalyst has less activity for conversion of propylene to 1-butanal (Figure 4.12 and 4.13). Unfortunately, after the catalytic run # 6 for both systems the formation of 1-butanal declined rapidly while propylene and other products increased. It is possible that the catalysts were some how deactivated.

4.4.3.2 IR Results

At the end of the catalysis course, the color of the used zeolite HY loaded $Rh(acac)(CO)_2$ catalysts changed from the initial gray to black and IR spectra in the range of carbonyl of the catalysts change from original pattern (see Figure 4.16 and Table 4.8).

The bands at 2103, 2034 and 2082 cm^{-1} were observed. No bridging CO bands are observed at lower frequencies, formation of rhodium clusters are neglected. The bands at 2103 and 2034 cm^{-1} are attributed to terminal rhodium dicarbonyl species and the band at 2082 cm^{-1} is possibly assigned to the terminal rhodium monocarbonyl species or

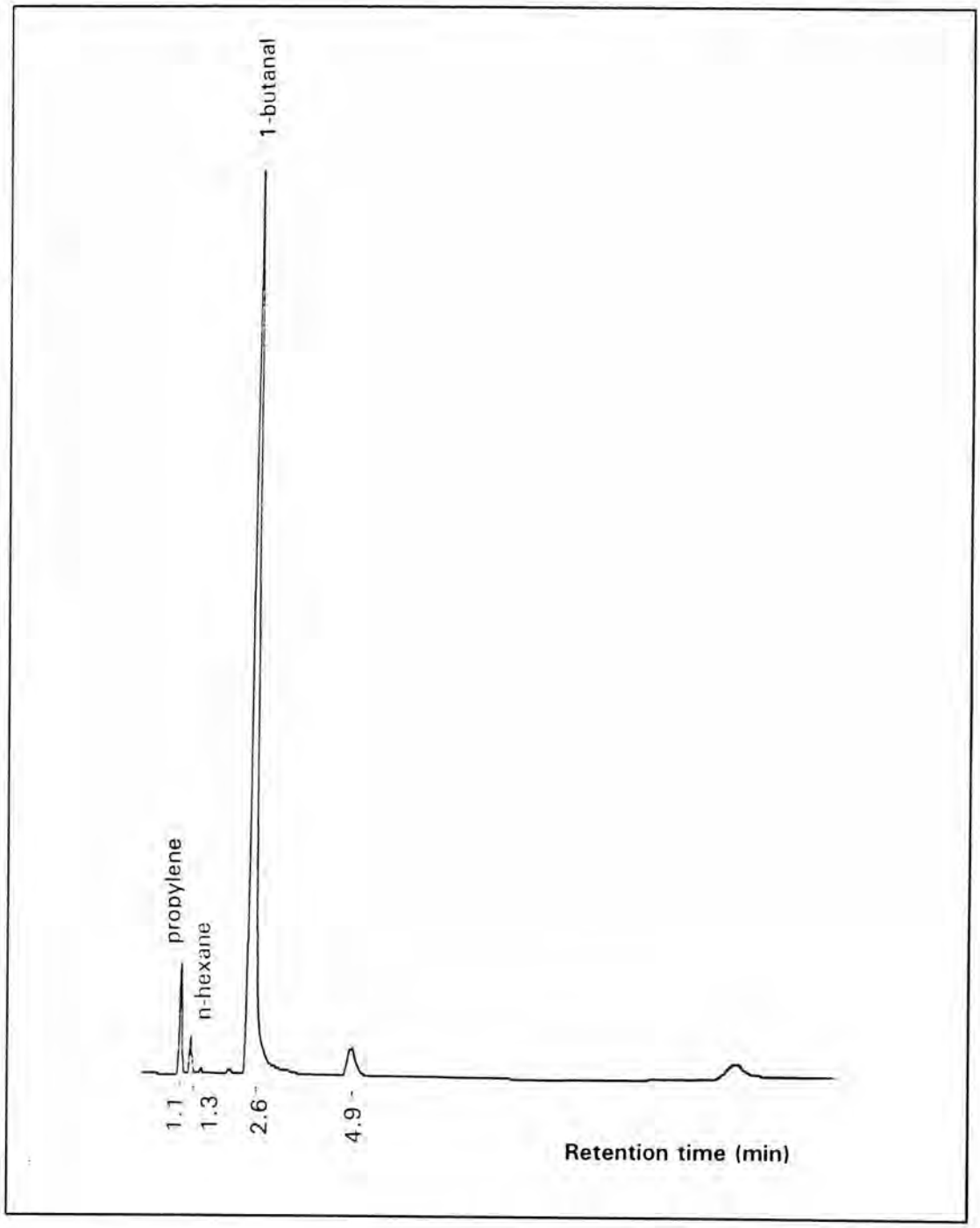

Figure 4.14 : Chromatogram of gas product from run # 5 of propylene hydroformylation with the zeolite HY loaded $Rh(acac)(CO)_2$ catalyst and $C_3:CO:H_2 = 1:2:6$.

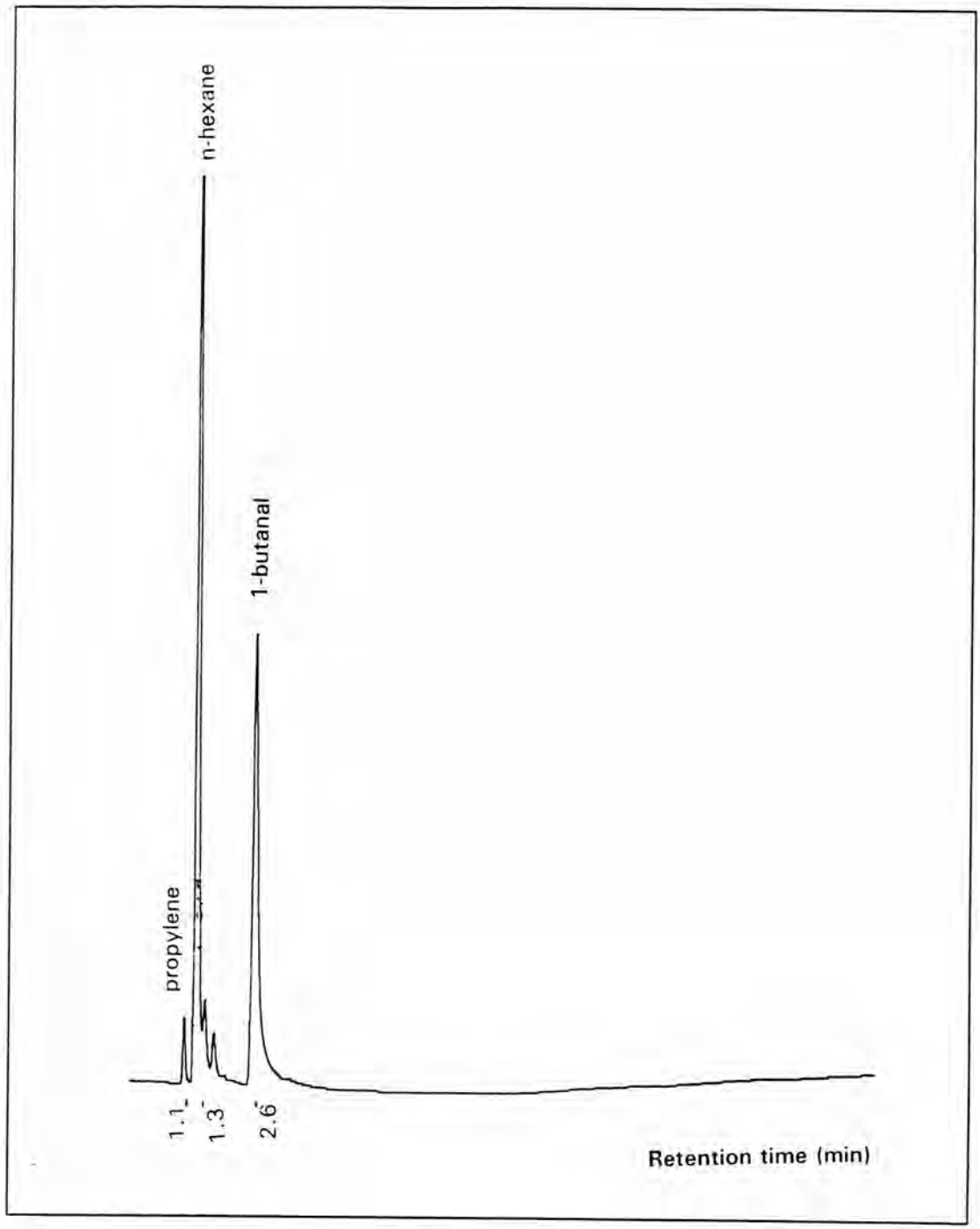

Figure 4.15 : Chromatogram of gas product from run # 5 of propylene hydroformylation with the zeolite NaY loded $Rh(acac)(CO)_2$ catalyst and $C_3:CO:H_2 = 1:2:6$.

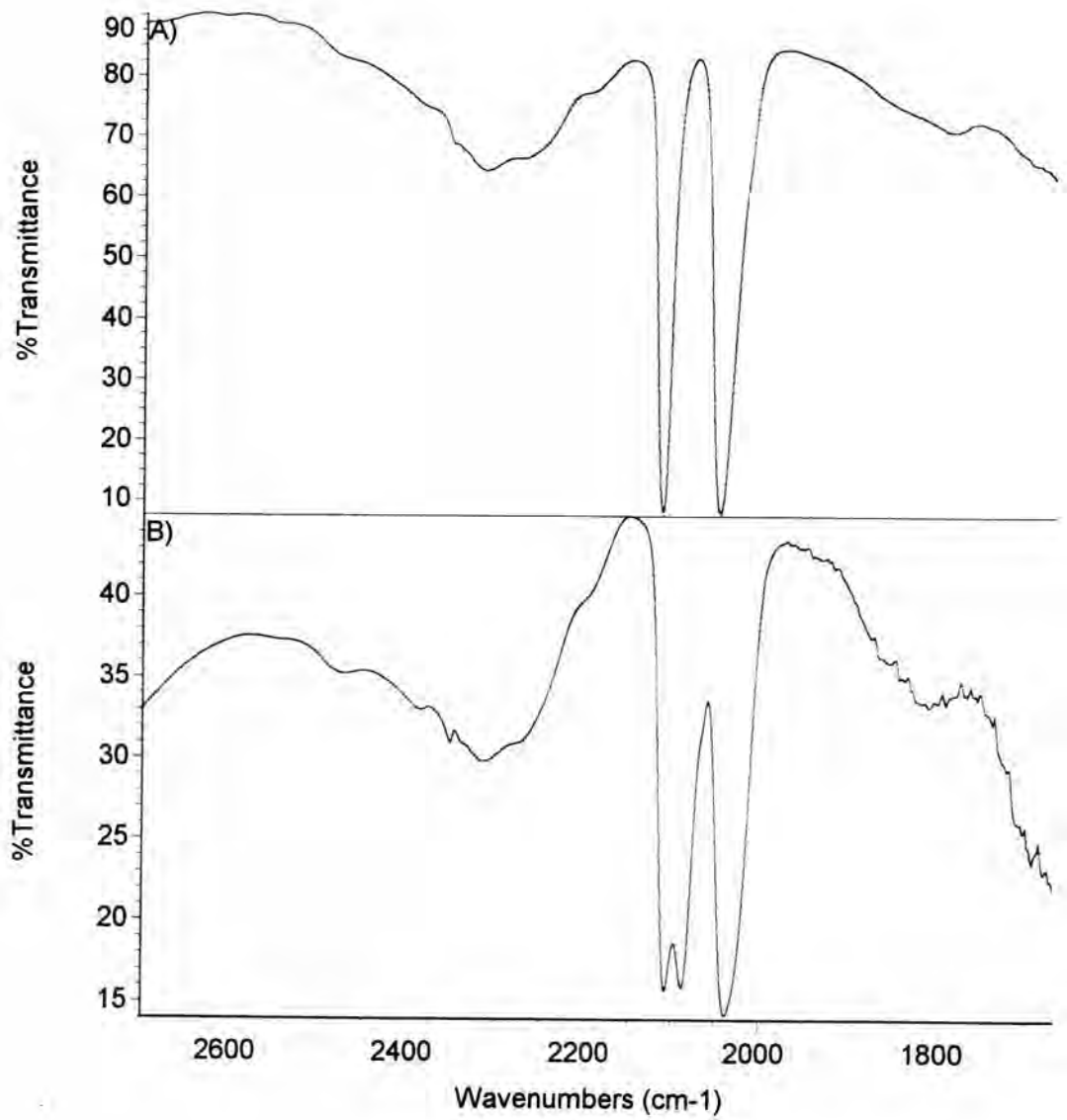

Figure 4.16 : IR data of the zeolite HY loaded $Rh(acac)(CO)_2$: A) Before catalysis; B) At the end of the propylene hydroformylation using C_3:CO:H_2 = 1:2:6.

Table 4.8 : IR data of the zeolite HY loaded $Rh(acac)(CO)_2$ before and after the propylene hydroformylation to Figure 4.16.

	ν_{CO} (cm^{-1})
Before catalysis	2110s, 2044s
After catalysis	2103s, 2082s, 2034s

rhodium hydride species.

The used zeolite NaY loaded $Rh(acac)(CO)_2$ catalysts after the run #6 with C_3:CO:H_2 = 1:2:6 changed in color from the initial greenish-gray to black and IR spectrum of carbonyl bands changed from the original spectra before the catalysis (Figure 4.17 and Table 4.9) as follows :

(i) The terminal carbonyl bands at 2103, 2039 and 2013 cm^{-1} disappear due to the decomposition of the zeolite anchored rhodium product, Z-O-$Rh(CO)_2$, and the unreacted $Rh(acac)(CO)_2$ in the zeolite NaY.

(ii) New carbonyl band at 1710 cm^{-1} was observed and this is the characteristic IR band of adsorbed 1-butanal in zeolite NaY. This result confirmed the formation of 1-butanal in trace amount which was adsorbed in zeolite pores and not detectable by GC till the catalytic run # 5.

(iii) New bands at 2092, 2060 and 1769 cm^{-1} were observed. The reported characteristic IR bands of rhodium carbonyl clusters are compiled

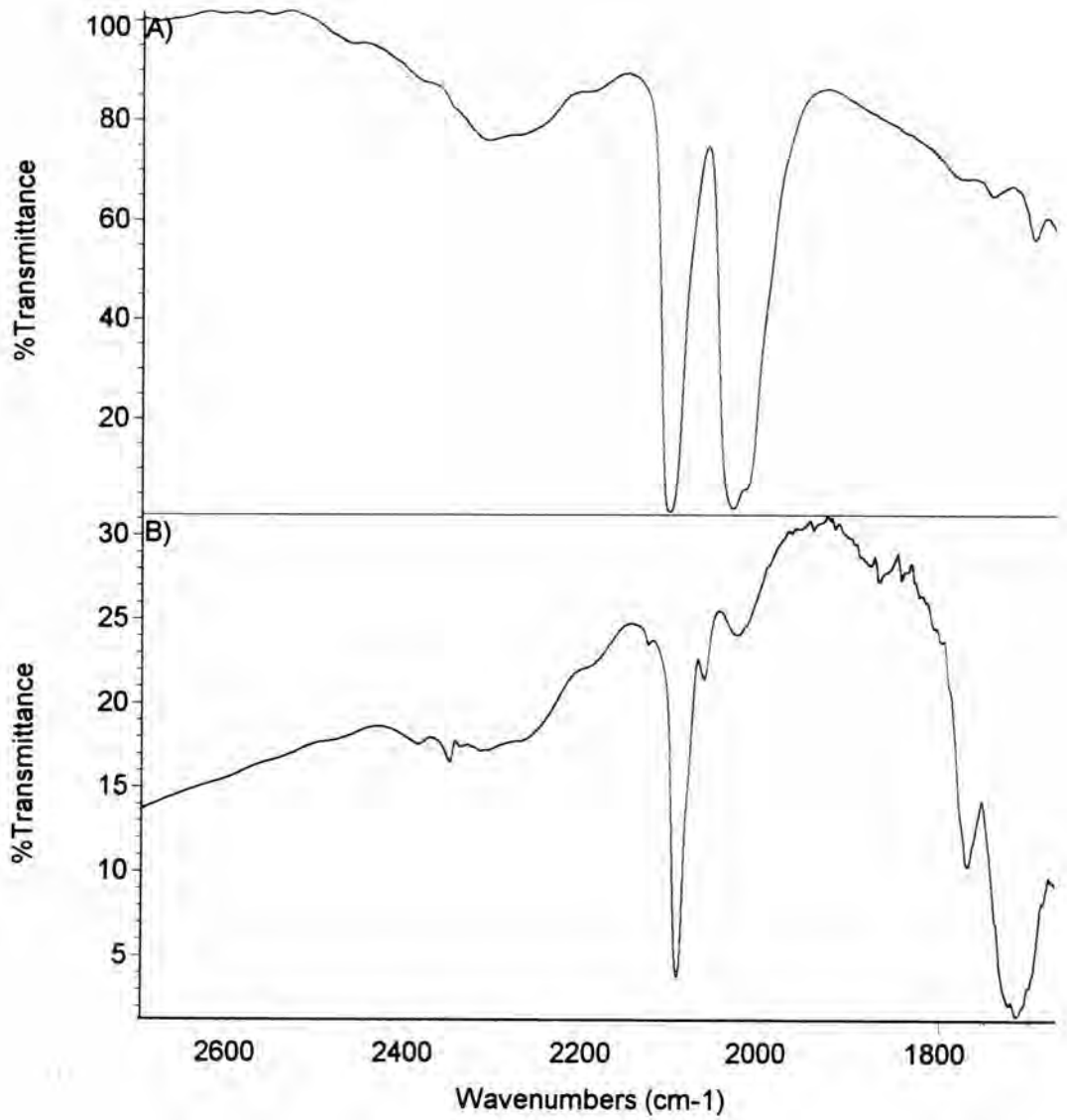

Figure 4.17 : IR data of the zeolite NaY loaded $Rh(acac)(CO)_2$: A) Before catalysis; B) At the end of the propylene hydroformylation using C_3:CO:H_2 = 1:2:6.

Table 4.9 : IR data of the zeolite NaY loaded $Rh(acac)(CO)_2$ before and after the propylene hydroformylation to Figure 4.17.

	ν_{CO} (cm^{-1})
Befor catalysis	2110s, 2044s
After catalysis	2103s, 2082s, 2034s

in Table 4.10. It suggested that the IR spectrum measured in this experiment (Figure 4.17) belongs to the face-bridging $Rh_6(CO)_{16}$ cluster immobilized in the zeolite supercage. The 2092 and 2060 cm^{-1} bands are assigned to the symmetric and asymmetric stretchings of the carbonyl while the 1769 cm^{-1} band is assigned to the characteristic bridging carbonyl of $Rh_6(CO)_{16}$.

Table 4.10 : Reported IR data of rhodium carbonyl clusters.

Cluster	ν_{CO} (cm^{-1})	Ref.
face-$Rh_6(CO)_{16}$/NaY	2098s, 2066w, 1760s	48-51
edge-$Rh_6(CO)_{16}$/NaY	2092s, 2060w,1830s	48
$Rh_4(CO)_{12}$/NaY	2082s, 2032s, 1876w, 1835s	48
$[Rh_{16}(CO)_{30}]^{-}/SiO_2$	2086w, 2040vs, 1834s	52
$[Rh_{12}(CO)_{30}]^{-2}/\gamma$-$Al_2O_3$	2086sh,2050vs, 2035sh, 1825w, 1797w	53
$[Rh_5(CO)_{15}]^{-}/\gamma$-$Al_2O_3$	2087w, 2050s, 2014s, 1820m	53

The relative intensities of carbonyl bands of Z-O-$Rh(CO)_2$ and unreacted $Rh(acac)(CO)_2$ decrease as the increace of the intensity of carbonyl bands of $Rh_6(CO)_{16}$. It indicates that Z-O-$Rh(CO)_2$ and the unreacted $Rh(acac)(CO)_2$ in the zeolite NaY can be converted to $Rh_6(CO)_{16}$ cluster under the catalytic condition. Among several researchers, Ichikawa et al,[48] and Davis et al,[49] found that $Rh^+(CO)_2$ on zeolite NaY was converted to $Rh_6(CO)_{16}$ in presence of CO and trace moisture. We suggest that this result is similar to the formation of $Rh_6(CO)_{16}$ from $Rh^+(CO)_2$ in zeolite NaY. $Rh_6(CO)_{16}$ clusters (< 10 Å) are accomodated within the zeolite supercages (12 Å inner radii), the structure of $Rh_6(CO)_{16}$ is shown in Figure 4.18.

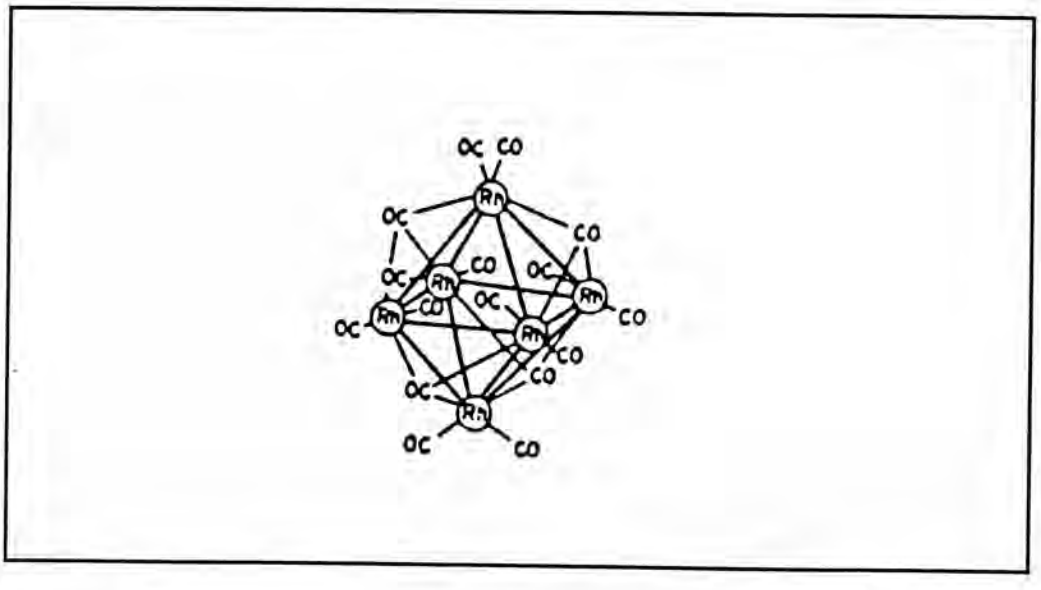

Figure 4.18 : Structure of $Rh_6(CO)_{16}$

It is known that $Rh_6(CO)_{16}$ cluster is inactive for hydroformylation of alkene and this is accounted for the deactivation of the zeolite NaY loaded $Rh(acac)(CO)_2$ catalyst at the end of the catalytic course.

4.4.3.3 XRD Data

XRD patterns of the used and unused zeolite HY loaded $Rh(acac)(CO)_2$ catalysts in Figure 4.19 show the change in structure of zeolite HY. This indicates that the structure of the zeolite HY collapsed to an amorphous material after prolonged period treatment. Due to a loss of the zeolite structure and its adsorption capability, this leads to no adsorbed butanal in zeolite HY. In contrast, XRD patterns of used zeolite NaY loaded $Rh(acac)(CO)_2$ catalyst (Figure 4.20) show no change from the original pattern of the unused catalyst. This indicates that the structure of zeolite NaY still retains due to its known higher stability than zeolite HY.

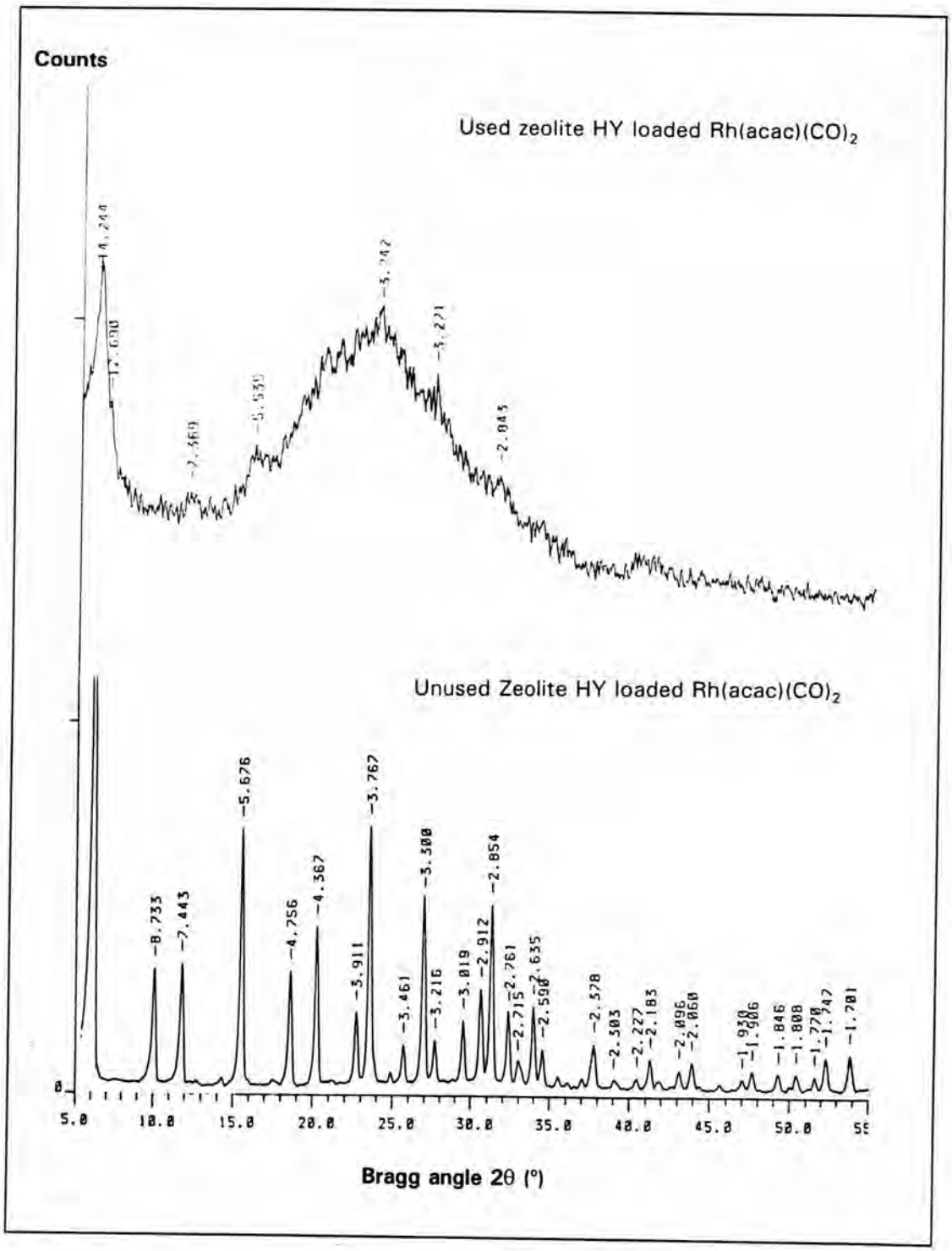

Figure 4.19 : XRD pattern of the zeolite HY loaded $Rh(acac)(CO)_2$ at the end of the propylene hydroformylation under C_3:CO:H_2 = 1:2:6.

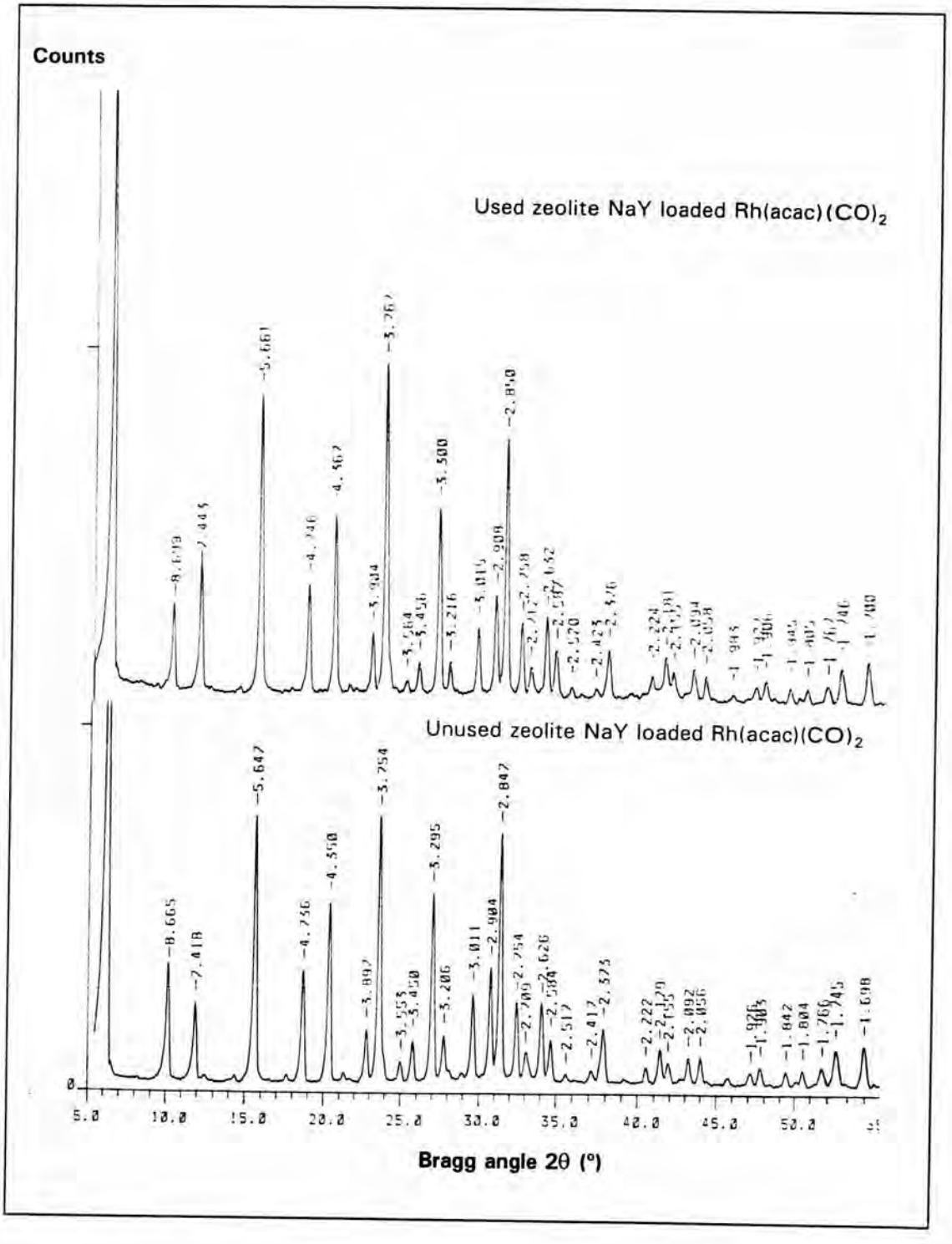

Figure 4.20 : XRD pattern of the zeolite NaY loaded $Rh(acac)(CO)_2$ at the end of the propylene hydroformylation under $C_3:CO:H_2 = 1:2:6$.

These catalysts are active for hydroformylation and can be recovered to work in propylene hydroformylation up to 5 times before they decomposed. The deactivation of the zeolites NaY and HY loaded $Rh(acac)(CO)_2$ lead to the formation of unreactive $Rh_6(CO)_{16}$ cluster in retained structure of zeolite NaY and a collapse of the zeolite HY structure, respectively.

4.4.4 Effect of C_3:CO:H_2 Ratio on Catalytic Activity

Various flow rates of C_3:CO:H_2 at ratio of 1:2:2, 1:2:6 and 1:4:2 produced changes in the product composition, the results of GC analysis shown in Table 4.11 and 4.12 were obtained from the utilization of the zeolite HY loaded $Rh(acac)(CO)_2$ and the zeolite NaY loaded $Rh(acac)(CO)_2$ as catalysts for 5 days. It should be noticed that the results were obtained after 5 time repeatedly of the reaction to accumulate as much products as possible.

Table 4.11 : GC analysis for propylene hydroformylation catalyzed by the zeolite HY loaded $Rh(acac)(CO)_2$ at different ratio of C_3:CO:H_2.

C_3:CO:H_2	*Rel. peak area (%)*					
	Propylene	**n-Hexene**	**1-Butanal**	**i Butanal**	**n-Butanol**	**Other products** *(Unidentified)*
1:2:6	7.74	2.33	87.43	0	0	2.50
1:2:2	50.01	1.17	6.52	0	4.08	38.22
1:4:2	33.33	9.03	8.94	6.02	15.85	12.60

Table 4.12 : GC analysis for propylene hydroformylation catalyzed by the zeolite NaY loaded $Rh(acac)(CO)_2$ at different ratio of C_3:CO:H_2.

C_3:CO:H_2	*Rel. peak area (%)*				
	Propylene	**n-Hexene**	**1-Butanal**	**i Butanal**	**Other products** *(unidentified)*
1:2:6	2.79	55.42	36.25	0	2.27
1:2:2	24.46	1.56	68.04	0	2.96
1:4:2	7.47	58.22	1.16	0.82	32.32

In propylene hydroformylation catalyzed by the zeolite HY loaded $Rh(acac)(CO)_2$ catalyst, it is found that the effect of composition of C_3:CO:H_2 on the activity of catalysts are as follows :

(i) The presence of excess CO leads to slight enhancement of the ratio of straight to branched butanal. A amount of 1-butanol is also obtained.

(ii) With the equal amount of CO and H_2, 1-butanal production increases while 1-butanol production decreases.

(iii) Excess H_2 leads to maximum aldehyde production.

On the other hand, the catalytic selectivity to aldehyde formation via hydroformation depends on the ratio of C_3:CO:H_2 in the order :

$$C_3:CO:H_2 = 1:2:6 >> 1:2:2 < 1:4:2$$

It is also found that the selectivity to 1-butanal depends on the ratio of CO:H_2, higher selectivity is provided by increase of CO:H_2 ratio. This shows that appropriate ratio of CO:H_2 is necessary to optimize the reaction condition. In this experiment, the highest selectivity to 1-butanal is obtained when C_3:CO:H_2 of 1:2:6 is used.

In propylene hydroformylation catalyzed by the zeolite NaY loaded $Rh(acac)CO)_2$ catalyst (see Table 4.12), it was found that the effect of composition of C_3:CO:H_2 on the activity of catalysts are as follows:

(i) Addition of excess CO leads to the lower activity of the catalyst for the hydroformylation, decreasing in the ratio of straight to branched butanal and increasing in other polar products.

(ii) Excess H_2 leads to the higher activity for the hydroformylation while the hydrogenation was observed as their major products.

(iii) In equivalent CO and H_2, the catalysts show higher selectivity formation of 1-butanal.

On the other hand, the selectivity to hydroformylation depends on the ratio of C_3:CO:H_2 which was in the order of :

$$C_3:CO:H_2 = 1:2:2 > 1:2:6 >> 1:4:2$$

In homogeneous system, it is known that the mechanism strongly depends on nature of solvents, metals, and ligands. In the zeolite media, it is found that the mechanism is affected by acidity of the zeolites, HY is much higher acidic than NaY. Therefore, the highest selectivity to 1-butanal is obtained when the C_3:CO:H_2 ratio for the HY system is 1:2:6 while is 1:2:2 for the NaY system.

4.5 Hydroformylation of 1-Hexene

4.5.1 Catalytic Activity of the Zeolite NaY Loaded Rh(acac)$(CO)_2$

The products in liquid phases from 1-hexene hydroformylation under condition of $CO:H_2 = 1:3$ at 1 atm and room temperature, analyzed by GC, are shown in Figures 4.21 to 4.23. After reaction time of 1 day, n-hexane and 1-heptanal were observed in little quantity in the liquid phase, moreover no observation of other products.

The products are not only 1-heptanal but also n-hexane and other unidentified products. This observation is indicative of 1-hexene hydrogenation competing with 1-hexene hydroformylation over the intrazeolite catalyst. Comparison of this result with experiment of hydroformylation of propylene, as described previously, suggests that increase in catalytic activity of the zeolite NaY loaded Rh(acac)$(CO)_2$ for hydroformylation of 1-hexene under the mild condition may be increased by the period of pre-treatment of the catalyst with the CO and H_2 gases.

The zeolite NaY loaded Rh(acac)$(CO)_2$ was pretreated with the synthesis gas (containing $CO:H_2 = 1:3$) for 5 days. The color of the catalyst changed from greenish-gray to brown-gray. As shown in Figure 4.24B, the intensities of the terminal carbonyl bands of Z-O-Rh$(CO)_2$ at 2103, 2039 cm^{-1} and unreacted Rh(acac)$(CO)_2$ in the zeolite at 2013 cm^{-1} drop off under this treatment while the new bands at 2092, 2062 and

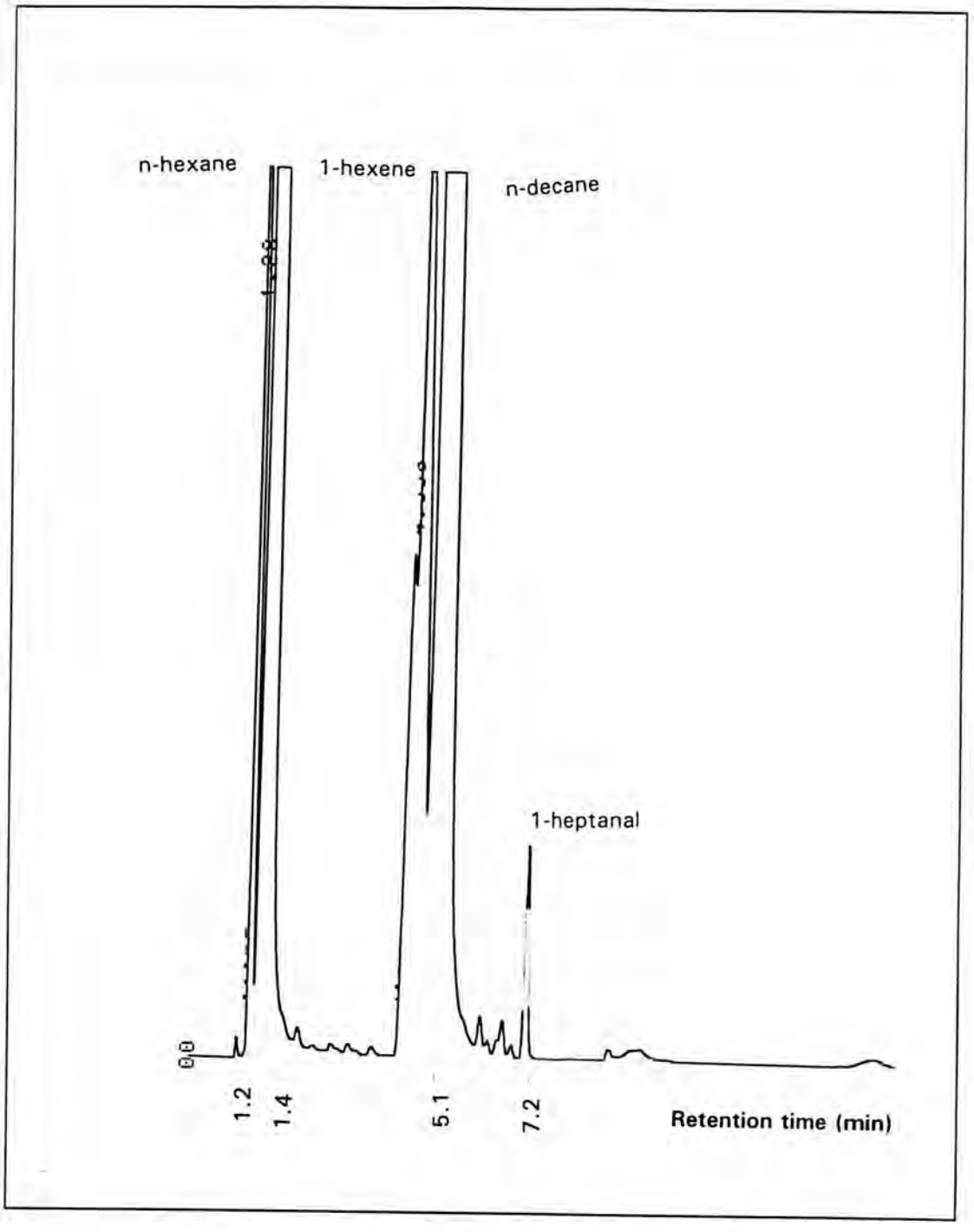

Figure 4.21 : Chromatogram of the liquid product from 1-hexene hydroformylation with the zeolite NaY loaded $Rh(acac)(CO)_2$ catalyst pretreated with $CO:H_2 = 1:3$ using the catalytic time for 4 days.

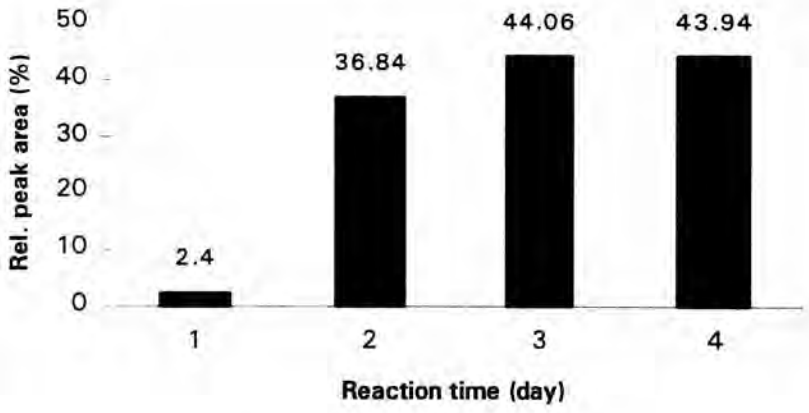

Figure 4.22 : Quantity of n-hexane in the liquid product from 1-hexene hydroformylation with the zeolite NaY loaded $Rh(acac)(CO)_2$ catalyst pretreated with $CO:H_2 = 1:3$.

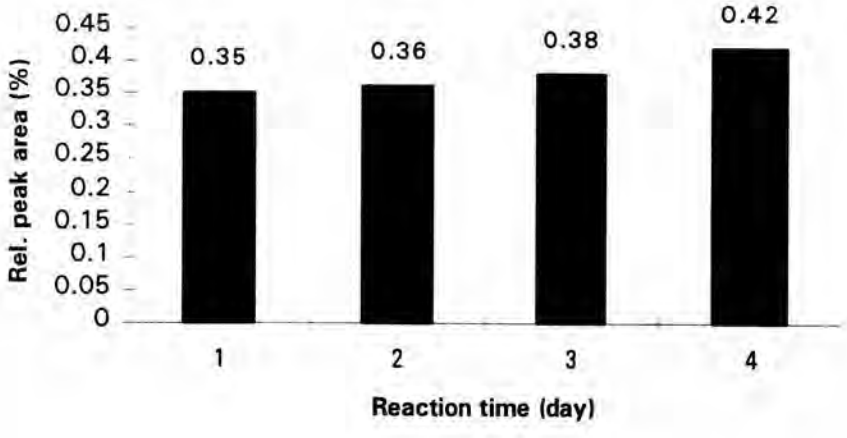

Figure 4.23 : Quantity of 1-heptanal in the liquid product from 1-hexene hydroformylation with the zeolite NaY loaded $Rh(acac)(CO)_2$ catalyst pretreated with $CO:H_2 = 1:3$.

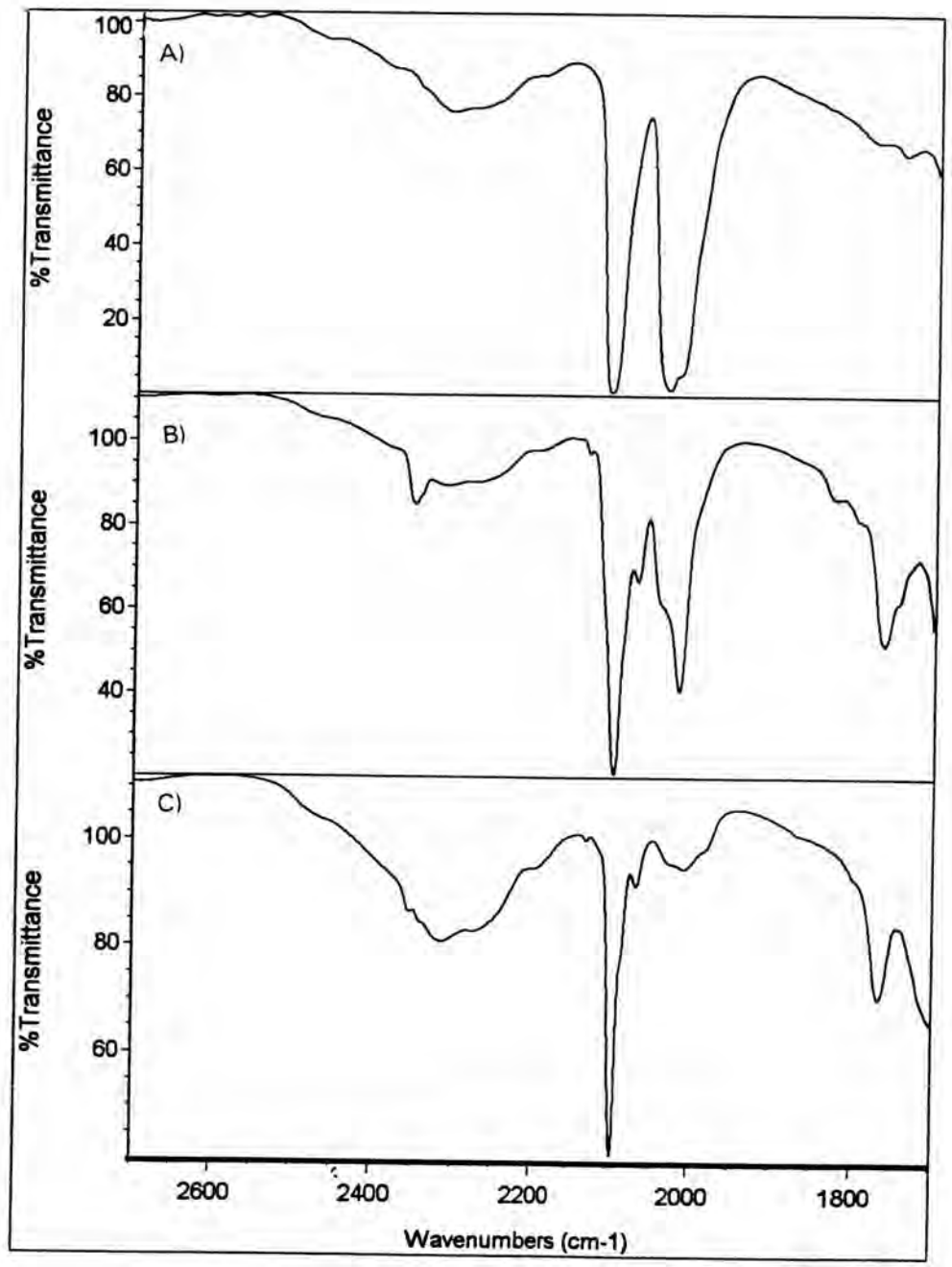

Figure 4.24 : IR spectra of the zeolite NaY loaded $Rh(acac)(CO)_2$ catalyst pretreated with $CO:H_2 = 1:3$: A = Initial; B = After pretreatment for 5 days; C = After the end of the 1-hexene hydroformylation.

1769 cm^{-1} appear. The results are assigned to the formation of the $Rh_6(CO)_{16}$ cluster within the zeolite supercage as found in propylene hydroformylation as reported in the previous section.

After the end of the 1-hexene catalytic course, the catalyst, removed from the reactor by filtration under N_2, was still brown-gray, with no indication of metallic Rh formation. As shown in Figure 4.24C, the infrared spectrum of the catalyst shows that $Rh_6(CO)_{16}$, some Z-O-$Rh(CO)_2$ and the unreacted $Rh(acac)(CO)_2$ were still present, and there was no evidence of other rhodium species. It indicates that these rhodium carbonyl species trapped in the zeolite cages.

The X-ray diffraction of the zeolite NaY loaded $Rh(acac)(CO)_2$ was measured after the run on hydroformylation of 1-hexene as shown in Figure 4.25. The XRD pattern indicates that the structure of zeolite is still unchanged or no collapse after catalysis.

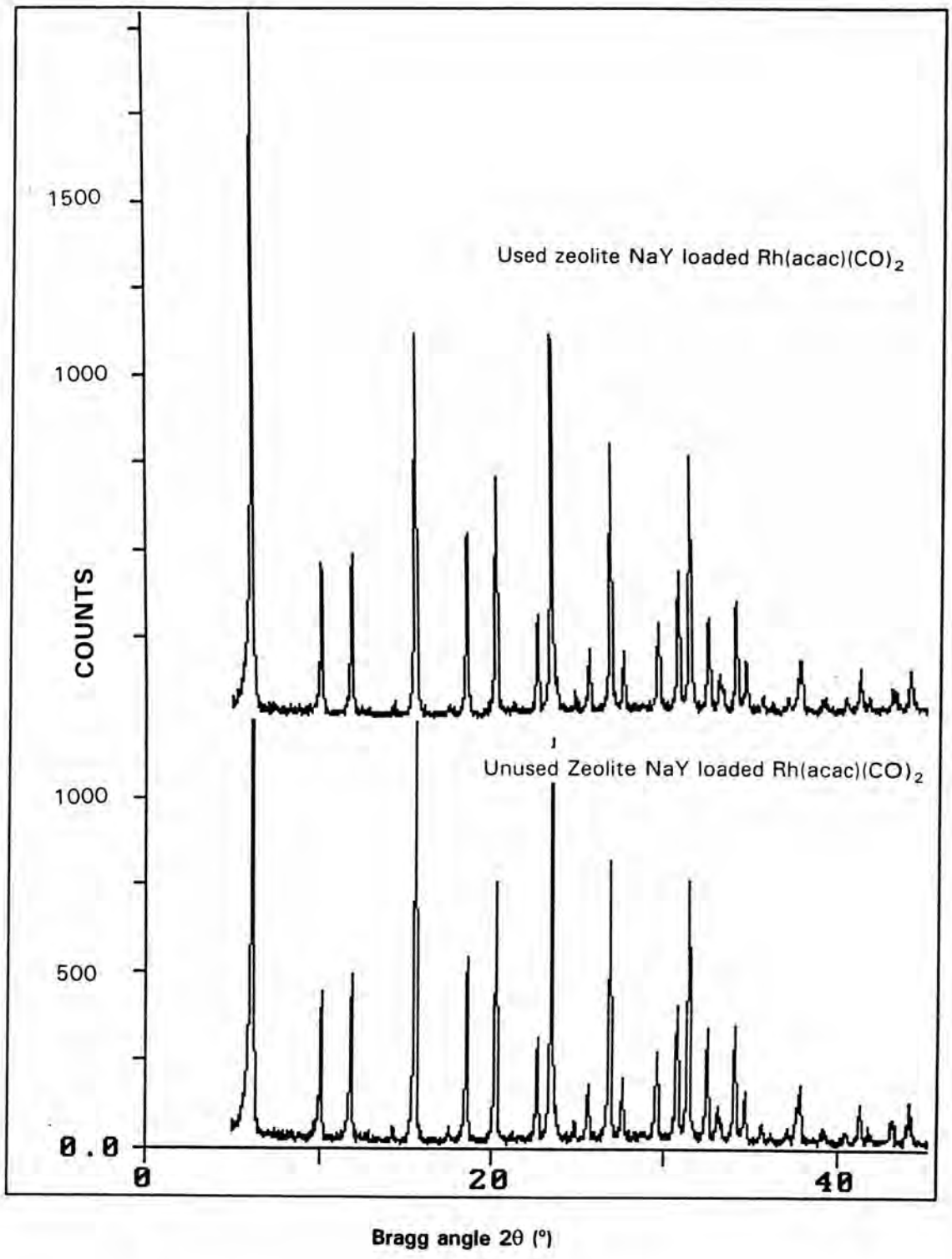

Figure 4.25 : XRD pattern of the zeolite NaY loaded $Rh(acac)(CO)_2$ catalyst at the end of the 1-hexene hydroformylation.

4.5.2 Catalytic Activity of the Zeolite HY Loaded $Rh(acac)(CO)_2$

The products in liquid phase from 1-hexene hydroformylation, catalyzed by the zeolite HY loaded $Rh(acac)(CO)_2$, under condition of $CO:H_2 = 1:3$ at 1 atm and room temperature are shown in Figures 4.26-4.28 1-Heptanal and n-hexane were observed in small quantity in the liquid phase whereas larger quantities of the other products were also observed.

The zeolite HY loaded $Rh(acac)(CO)_2$ was pre-treated with the synthesis gas (containing $CO:H_2 = 1:3$) for 5 days. Before adding 1-hexene and after the pre-treatment, the color of the solid sample was still gray and also the infrared spectrum of Z-O-$Rh(CO)_2$ was still unchanged (Figure 4.29).

The trace amount of 1-heptanal product was observed, which indicates that only a small amount of active site Z-O-$Rh(CO)_2$ was derived.

After this catalytic test, the XRD pattern, shown in Figure 4.30, indicates that the structure of zeolite still retains.

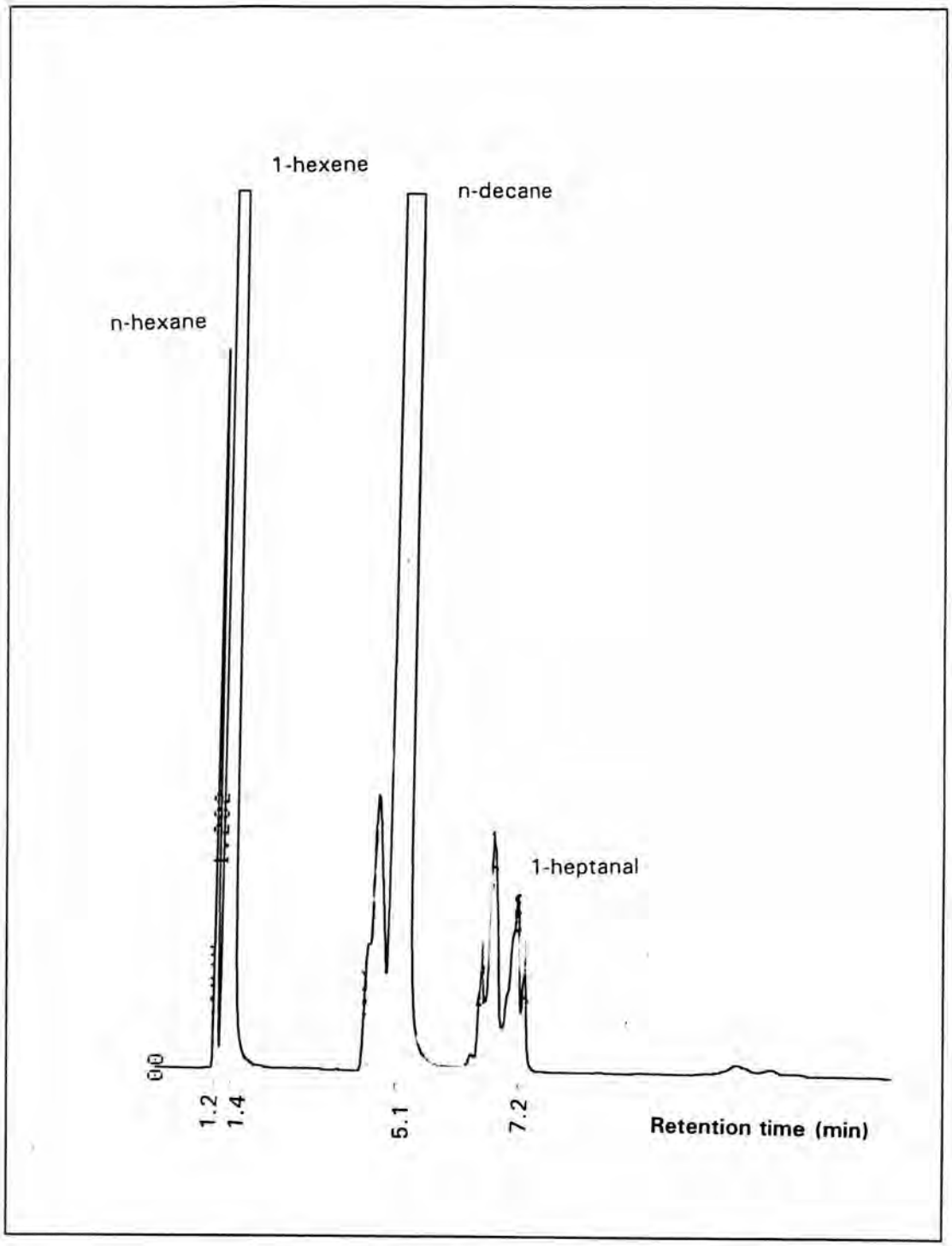

Figure 4.26 : Chromatogram of the liquid product from 1-hexene hydroformylation with the zeolite HY loaded $Rh(acac)(CO)_2$ catalyst pretreated with $CO:H_2 = 1:3$ using the catalytic time for 4 days.

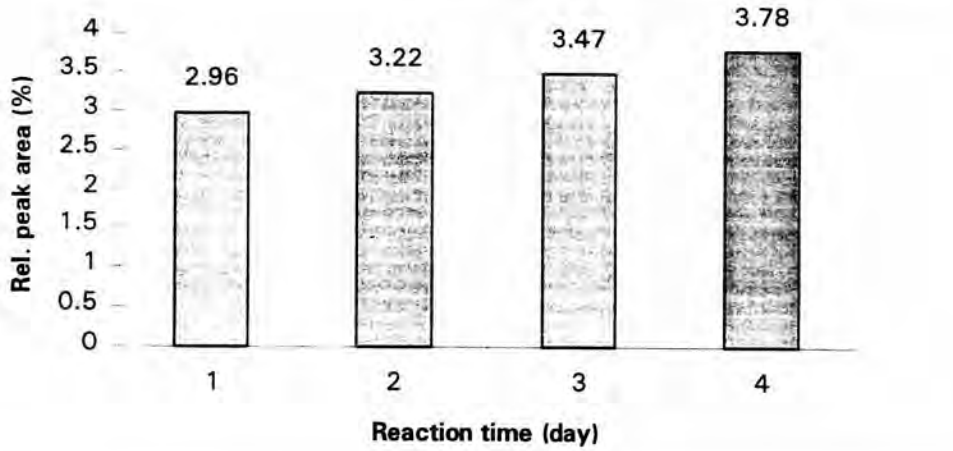

Figure 4.27: Quantity of n-hexane product in liquid phase from 1-hexene hydroformylation with the zeolite HY loaded $Rh(acac)(CO)_2$ catalyst pretreated with $CO:H_2 = 1:3$.

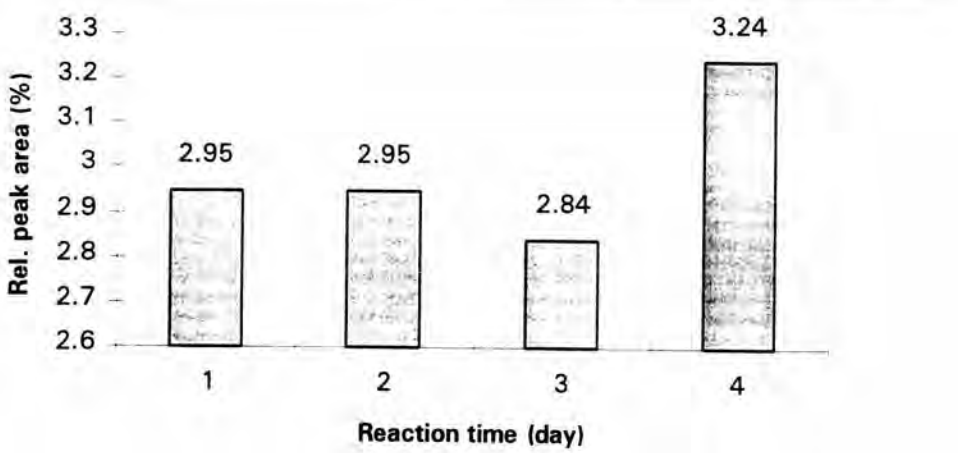

Figure 4.28 : Quantity of 1-heptanal product in liquid phase from 1-hexene hydroformylation with the zeolite HY loaded $Rh(acac)(CO)_2$ catalyst pretreated with $CO:H_2 = 1:3$.

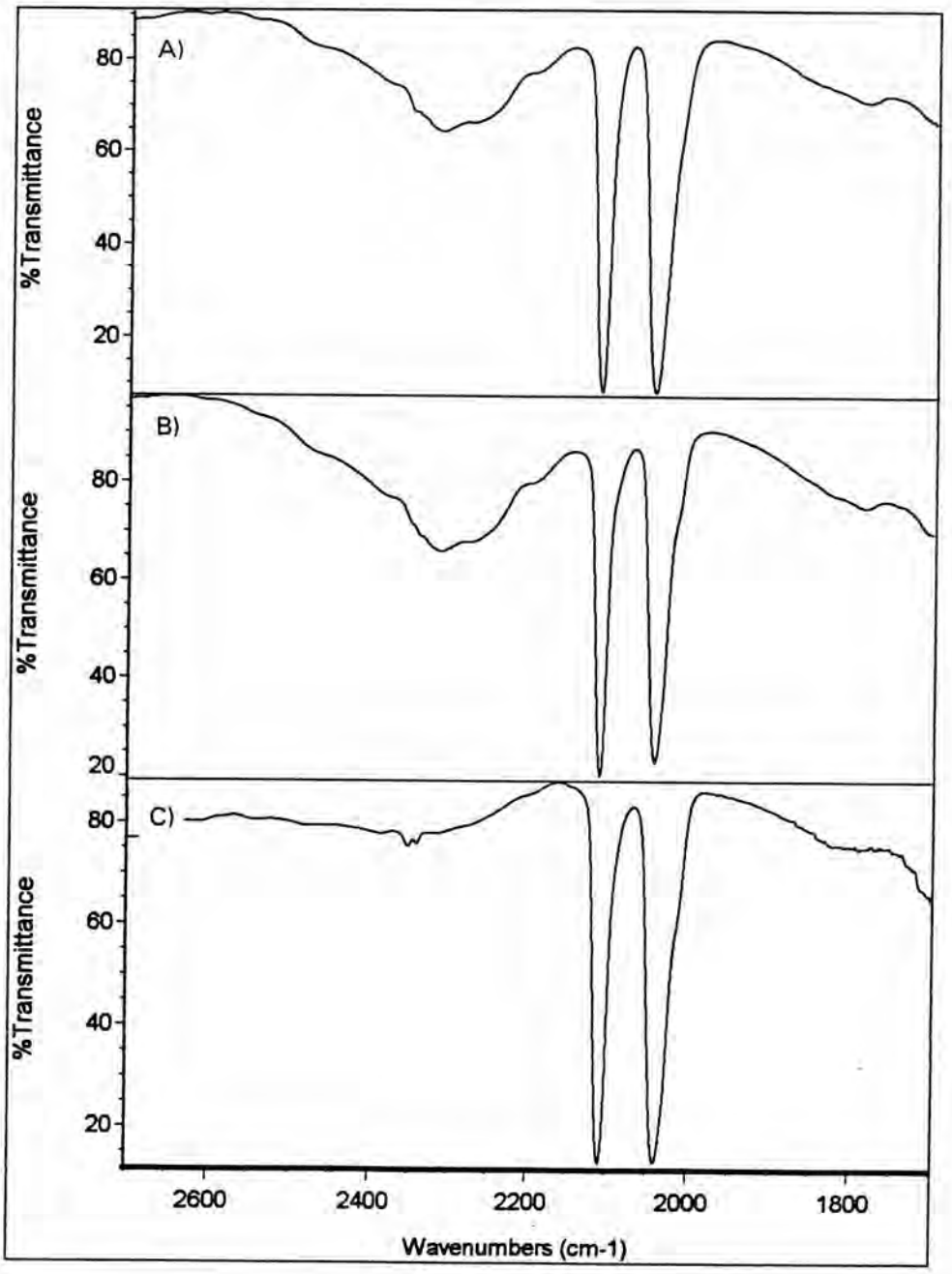

Figure 4.29 : IR spectra of the zeolite HY loaded $Rh(acac)(CO)_2$ catalyst pretreated with $CO:H_2 = 1:3$: A = Initial; B = After pretreatment for 5 days; C = After the end of the 1-hexene hydroformylation.

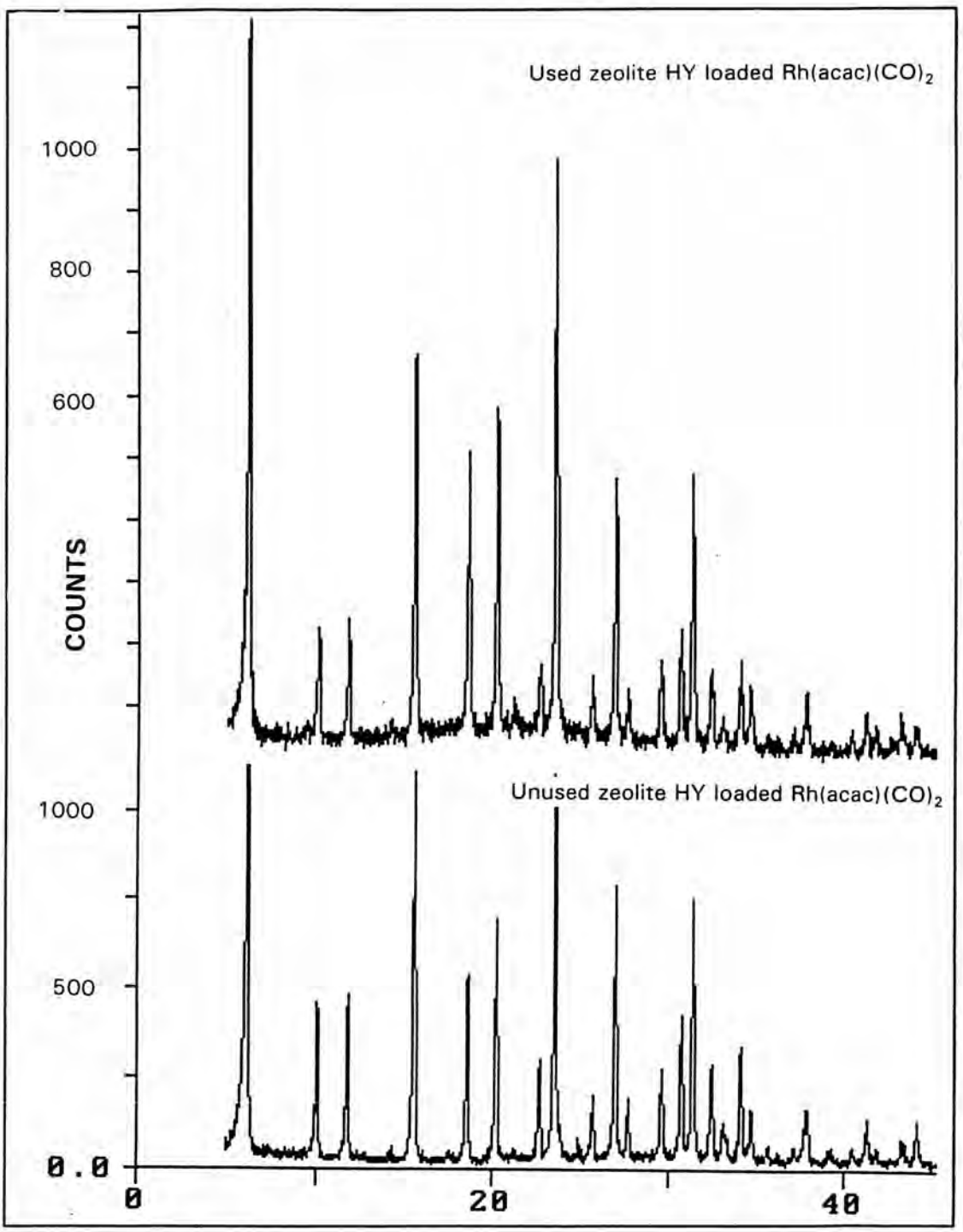

Figure 4.30 : XRD patterns of the zeolite HY loaded $Rh(acac)(CO)_2$ catalyst at the end of the 1-hexene hydroformylation.

4.6 Conclusion and Suggestion

Zeolite Y (SiO_2:Al_2O_3=4.6) was successfully synthesized by the method developed in this work. Slurry of nucleation centers with composition of $16.2Na_2O:1.2Al_2O_3:15SiO_2:640H_2O$ was aged for at least 4 days prior to mixing with the reactant mixture of $1.9Na_2O:Al_2O_3:6SiO_2:100H_2O$. The obtained milky solution was crystallized at 100 °C for 40-65 h. Zeolite HY was carried out via ammonium exchange with the solution of ammonium chloride and subsequent deammination (removal of ammonia) at elevated temperature.

The $Rh(acac)(CO)_2$ precursor can be anchored to the internal surface of the zeolite framework in either zeolites NaY and HY at room temperature. The precursor reacted completely with the proton in the zeolite HY while it reacted incompletely with the sodium ions in the zeolite NaY. This result shows that the protons of zeolite Y are more reactive than the sodium ions for anchoring reaction of $Rh(acac)(CO)_2$ to the zeolite surface. The zeolite NaY loaded $Rh(acac)(CO)_2$ decomposed at 80 °C in vacuo while zeolite HY loaded $Rh(acac)(CO)_2$ decomposed at 300 °C in vacuo. This result shows that the zeolite HY supported caatalyst is more thermally stable than the zeolite NaY supported catalyst.

The zeolites NaY loaded $Rh(acac)(CO)_2$ and HY loaded $Rh(acac)(CO)_2$ can act as hydroformylation catalysts for producing linear aldehyde from

propylene and 1-hexene at ambient pressure and temperature. It was found that the zeolite HY loaded $Rh(acac)(CO)_2$ is more catalytically active than the zeolite NaY loaded $Rh(acac)(CO)_2$. The decomposition of the zeolite NaY leads to the formation of unreactive $Rh_6(CO)_{16}$ cluster in retained structure of zeolite NaY while the decomposition of the zeolite HY loaded $Rh(acac)(CO)_2$ is due to collapse of the zeolite HY structure.

The suggestion for future work :

1) Synthetic zeolite Y is recommended to be charecterized by the other method (etc. SEM, DTA).

2) Zeolite HY loaded $Rh(acac)(CO)_2$ and zeolite NaY loaded $Rh(acac)(CO)_2$ are recommended to be structurally characterized by EXAFS spectroscopy.

3) Hydroformylation system is recommended to be improved by using higher temperature and pressure.

4) Separation of the products from zeolite is recommended to be improved by using vacuum distillation at high temperatrure.

5) Unidentified products in propylene and 1-hexene hydroformylation systems recommended to be identified by GC/MS technique. This work should have been done in this project but all mechines located at the university are not in-service.